Genome-wide histone methylation profile for heart failure

Ruri Kaneda[1,2], Shuji Takada[1], Yoshihiro Yamashita[1], Young Lim Choi[1], Mutsuko Nonaka-Sarukawa[2], Manabu Soda[1], Yoshio Misawa[3], Tadashi Isomura[4], Kazuyuki Shimada[2] and Hiroyuki Mano[1,5,*]

Divisions of [1]Functional Genomics, Jichi Medical University, Tochigi 329-0498, Japan
[2]Cardiovascular Medicine, Jichi Medical University, Tochigi 329-0498, Japan
[3]Cardiovascular Surgery, Jichi Medical University, Tochigi 329-0498, Japan
[4]Hayama Heart Center, Kanagawa 240-0116, Japan
[5]CREST, Japan Science and Technology Agency, Saitama 332-0012, Japan

Epigenetic alterations are implicated in the development of cardiac hypertrophy and heart failure, but little is known of which epigenetic changes in which regions of the genome play such a role. We now show that trimethylation of histone H3 on lysine-4 (K4TM) or lysine-9 (K9TM) is markedly affected in cardiomyocytes in association with the development of heart failure in a rat disease model. High-throughput pyrosequencing performed with ChIP products for K4TM or K9TM prepared from human left ventricular tissue with retained or damaged function also revealed that protein-coding genes located in the vicinity of K4TM marks differ between functional and disabled myocytes, yet both sets of genes encode proteins that function in the same signal transduction pathways for cardiac function, indicative of differential K4TM marking during the development of heart failure. However, K9TM mark-profile was less dependent on the disease status compared to that of K4TM. Our data collectively reveal global epigenetic changes in cardiac myocytes associated with heart failure.

Introduction

A variety of conditions, including pressure or volume overload in the cardiovascular system and remodeling of the left ventricle of the heart after ischemic damage, result in heart failure, which is characterized by a reduction in contractile ability and a decrease in the number of viable myocytes in the heart (James *et al.* 2000). Treatment of heart failure remains problematic, and this condition is thus still one of the leading causes of human death (Braunwald 1997).

Epigenetic status has been linked to cardiac hypertrophy and heart failure. The histone acetyltransferase activity of CREB-binding protein (CBP) and p300 is thus required for the induction of hypertrophic changes in cardiac muscle cells by phenylephrine (Gusterson *et al.* 2003). Consistent with this observation, inhibition of histone deacetylase (HDAC) activity results in an increase in the size of cardiac muscle cells (Iezzi *et al.* 2004). Furthermore, HDACs of class II (HDAC4, -5, -7, and -9) suppress cardiac hypertrophy in part by binding to and inhibiting the activity of myocyte enhancer factor 2 (Zhang *et al.* 2002). Induction of the atrial natriuretic peptide gene is associated with acetylation of histones (H3 and H4) located in the 3′ untranslated region of the gene (Kuwahara *et al.* 2001). Histones bound to the β-myosin heavy chain gene have also been shown to be targeted by histone acetyltransferases in cardiomyocytes (Zhang *et al.* 2002). Moreover, dynamic regulation of other histone modifications has been demonstrated in cardiac myocytes (Illi *et al.* 2005; Bingham *et al.* 2007).

It remains to be established, however, (i) which epigenetic marks are dysregulated in association with heart failure *in vivo*, (ii) which regions of the human genome are susceptible to such epigenetic changes, and (iii) how epigenetic dysregulation affects the expression of protein-coding or other genes. To address these issues, we have now studied an animal model of congestive heart failure (CHF), the Dahl salt-sensitive rat (Rapp *et al.* 1989), and found that two histone modifications are markedly affected in cardiac myocytes during the development of CHF. We further confirmed our findings in human left ventricular (LV) myocytes with the use of chromatin immunoprecipitation

Communicated by: Kohei Miyazono
**Correspondence*: hmano@jichi.ac.jp

DOI: 10.1111/j.1365-2443.2008.01252.x

(ChIP) coupled to pyrosequencing. Our results have revealed dynamic histone modifications in the vicinity of a subset of protein-coding genes in the human genome, which directly participate in regulation of the contraction of cardiac myocytes.

Results

Histone modifications in the heart of Dahl rats

We prepared LV myocytes from Dahl salt-sensitive rats, which are genetically intolerant to excessive salt intake (Rapp *et al.* 1989). A high-sodium diet thus induces systemic hypertension and cardiac hypertrophy in Dahl rats within a few weeks. These changes are followed within a few months by the development of CHF and death. We isolated cardiac myocytes from rats with CHF (fed a high-sodium diet) as well as from age-matched animals with a normal heart (fed a low-sodium diet), and we subjected these cells to ChIP with antibodies to acetylated histone H3 (H3Ac), acetylated histone H4 (H4Ac), histone H3 dimethylated on lysine-4 (K4DM), histone H3 trimethylated on lysine-4 (K4TM), histone H3 dimethylated on lysine-9 (K9DM), histone H3 trimethylated on lysine-9 (K9TM), histone H4 trimethylated on lysine-20 (K20TM), or histone H3 dimethylated on lysine-27 (K27DM). The ChIP products as well as cRNA prepared from the normal or failed hearts were then individually subjected to hybridization with high-density oligonucleotide microarrays (Affymetrix Rat Genome 230 2.0 GeneChip) originally developed for expression profiling of rat genes.

Pearson's correlation coefficient for the signal intensity of all probe sets with a "Present" call (by Affymetrix GCOS software) in the normal heart (n = 13 914) was 0.873 in the cRNA hybridizations for normal and failed hearts (Fig. 1), indicative of a strong correlation in the expression level of most genes between the two samples. Consistent with this observation, the signal intensity for all probe sets with a positive value in the H3Ac ChIP products from the normal heart (n = 12 027) was highly correlated between these products from normal and failed hearts (r = 0.724). A similar strong correlation between the two groups was observed for H4Ac.

Unexpectedly, however, despite the strong correlation (r = 0.856) apparent for K4DM, only a weak negative correlation (r = –0.097) was detected for the K4TM mark between normal and failed hearts, indicative of marked differences in the associated gene sets. Similarly, although a strong correlation was observed for K9DM (r = 0.558), a weak negative correlation (r = –0.251) was apparent for K9TM. Hybridization levels were positively correlated between normal and failed hearts for K20TM and K27DM.

Thus, among the epigenetic marks examined, K4TM and K9TM were the histone modifications most affected in heart failure. Although differences in functional roles and genomic distributions between K4DM and K4TM have been described (Santos-Rosa *et al.* 2002; Bernstein *et al.* 2005), little has been known of such differential roles for the methylation level of lysine-9 of histone H3.

K4TM and K9TM profiles in the human heart

We next attempted to identify the genomic regions associated with the K4TM and K9TM marks in human cardiac myocytes. ChIP products for K4TM or K9TM were prepared from a mixture of LV tissue specimens from four individuals with retained pumping function [LV ejection fraction (EF) of 65.5 ± 7.6%, mean ± SD] or from four individuals with CHF (LVEF of 19.8 ± 5.7%) caused by dilated cardiomyopathy (Table 1). The ChIP

Table 1 Clinical characteristics of the subjects who provided specimens for the study

	Sample ID	Disease	Age (years)	Sex	LVEF (%)
HighEF	PM 8	HVD (MSR, ASR)	59	F	65
	PM12	HVD (MSR)	73	F	58
	PM13	HVD (MS)	55	F	76
	PM14	HVD (MS)	62	F	63
CHF	LV13	DCM	52	M	17
	LV14	DCM	55	M	25
	LV18	DCM	57	M	13
	LV20	DCM	64	F	24

HVD, heart valvular disease; MS(R), mitral stenosis (and regurgitation); ASR, aortic stenosis and regurgitation; DCM, dilated cardiomyopathy; F, female; M, male.

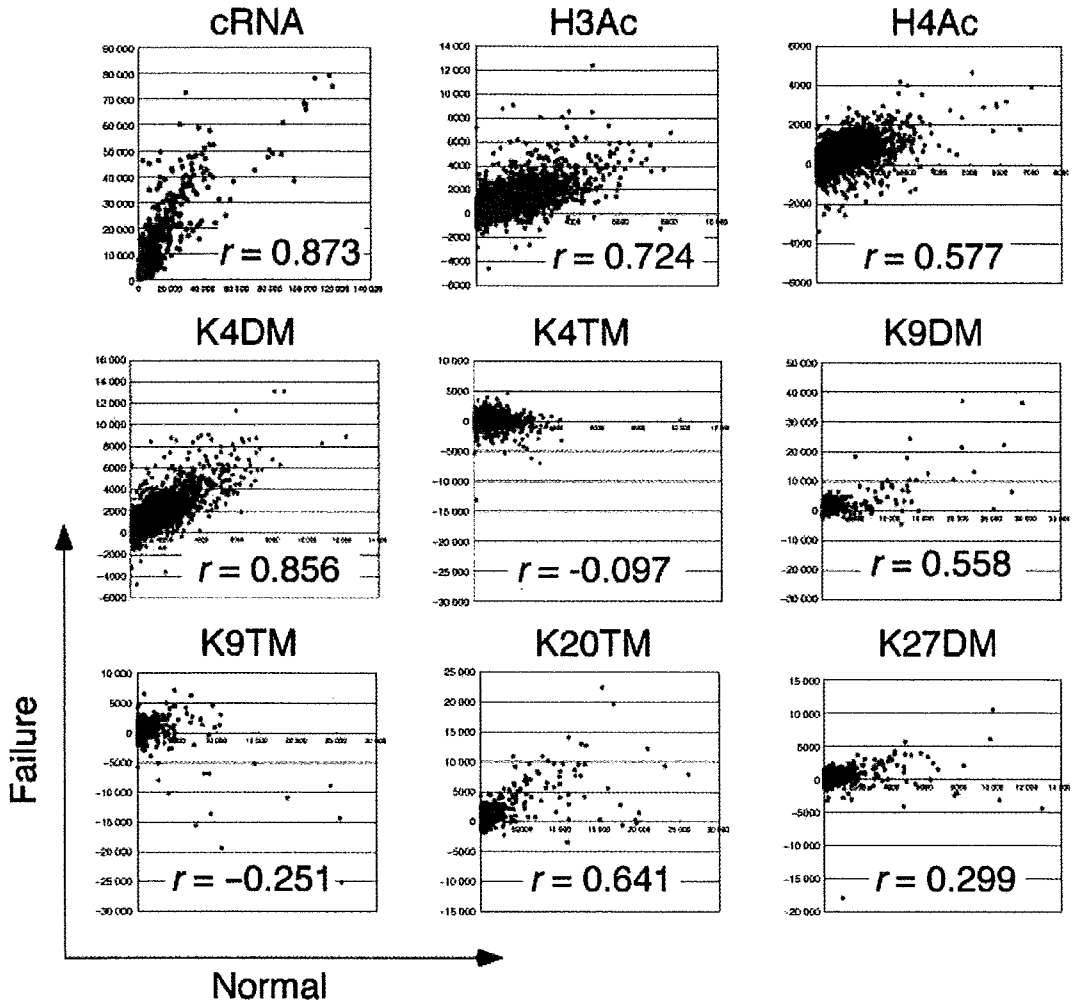

Figure 1 Comparison of epigenetic profiles between normal and failed rat hearts. The expression level of each probe set on oligonucleotide microarrays was compared between total cRNA from normal (*x* axis) or failed (*y* axis) hearts by calculation of Pearson's correlation coefficient (*r*). ChIP-on-chip data for H3Ac, H4Ac, K4DM, K4TM, K9DM, K9TM, K20TM, and K27DM are similarly compared.

products were subjected to pyrosequencing with the Genome Sequencer 20 system (Roche). In this "ChIP-to-seq" experiment, 96 069, 95 596, 116 267, and 96 734 reads were obtained for the K4TM products for specimens with retained LV ejection fraction (HighEF), the K4TM products for CHF, the K9TM products for HighEF, and the K9TM products for CHF, respectively. After quality-filtering, we isolated an average of 36 279 reads per sample, for each of which a single hit with a highest matching score was identified in the human genome sequence (the hg18 assembly of the Genome Bioinformatics Group, University of California at Santa Cruz) (Table S1 in Supporting Information). We thus focused on these reads for further analysis.

Many regions of the genome were identified in which multiple sequence reads mapped closely to each other. We therefore defined a "cluster" as a group of sequence reads localized within a distance of 1 kbp in the human genome (Fig. 2A). A total of 94 202 clusters was identified for all four samples, and 18 725 of these clusters, referred to as "high clusters," contained ≥ 2 sequence reads in ≥ 1 sample (see Table S2 in Supporting Information).

We then examined histone modification at the high clusters for specificity of the epigenetic mark (K4TM or

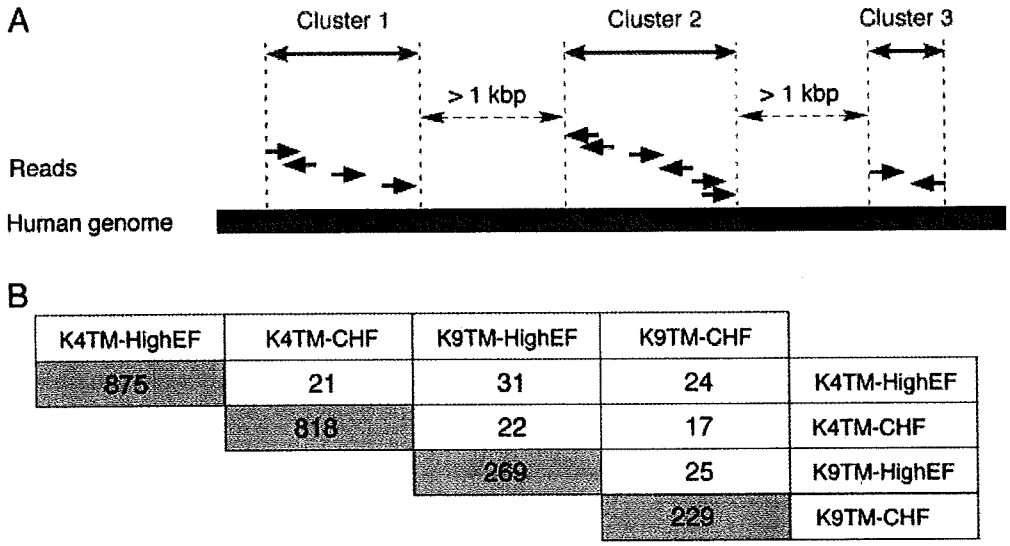

Figure 2 High clusters in K4TM and K9TM ChIP-to-seq data. (A) Groups of sequence reads that map to the human genome within a distance of 1 kbp are defined as "clusters," which are further denoted as "high clusters" when the read number in the cluster is ≥ 2 in ≥ 1 sample. (B) Numbers of high clusters with a read number of ≥ 5 for K4TM or K9TM in HighEF or CHF samples (shaded boxes). The numbers of such clusters shared between any pair of samples is also indicated (open boxes).

Table 2 Disease-specific high clusters

Mark	Characteristics of high clusters	Total number of high clusters	Number of high clusters close to RefSeq genes	Number of high clusters close to CpG islands
K4TM	HighEF ≥ 5, CHF ≤ 1	836	407	129
	HighEF ≤ 1, CHF ≥ 5	786	432	163
K9TM	HighEF ≥ 5, CHF ≤ 1	220	75	18
	HighEF ≤ 1, CHF ≥ 5	196	69	10

K9TM) and disease status (HighEF or CHF). Among the high clusters, 875 had ≥ 5 reads in the K4TM product for HighEF, 818 had ≥ 5 reads in the K4TM product for CHF, 269 had ≥ 5 reads in the K9TM product for HighEF, and 229 had ≥ 5 reads in the K9TM product for CHF (Fig. 2B). Only a few dozen of such high clusters were shared between any pair of samples, indicating the existence of disease-specific as well as methylation site-specific epigenetic profiles. Therefore, despite the heterogeneity in the cause of CHF (sustained systemic hypertension or dilated cardiomyopathy), both the Dahl rat and human data sets revealed a marked difference in the K4TM and K9TM epigenetic profiles between normal and failed hearts. Such specificity is further visualized for human chromosome 1 in Fig. S1 in Supporting Information. In contrast, the profile of read number per cluster was similar among the four groups of human ChIP products (see Fig. S2 in Supporting Information).

Genes mapped closely to disease-dependent clusters

We then isolated disease status-specific high clusters from the data set. A total of 836 high clusters was found to contain ≥ 5 reads in the K4TM products for HighEF but ≤ 1 read in those for CHF (HighEF-specific K4TM clusters); 407 RefSeq genes mapped to within ≤ 5 kbp of these clusters (Table 2). Similarly, 786 high clusters were found to be specific for K4TM and CHF (≤ 1 read in the K4TM products for HighEF but ≥ 5 reads in those for CHF). Smaller numbers of disease-dependent clusters were identified for the K9TM mark (220 HighEF-specific and 196 CHF-specific). These disease-dependent clusters

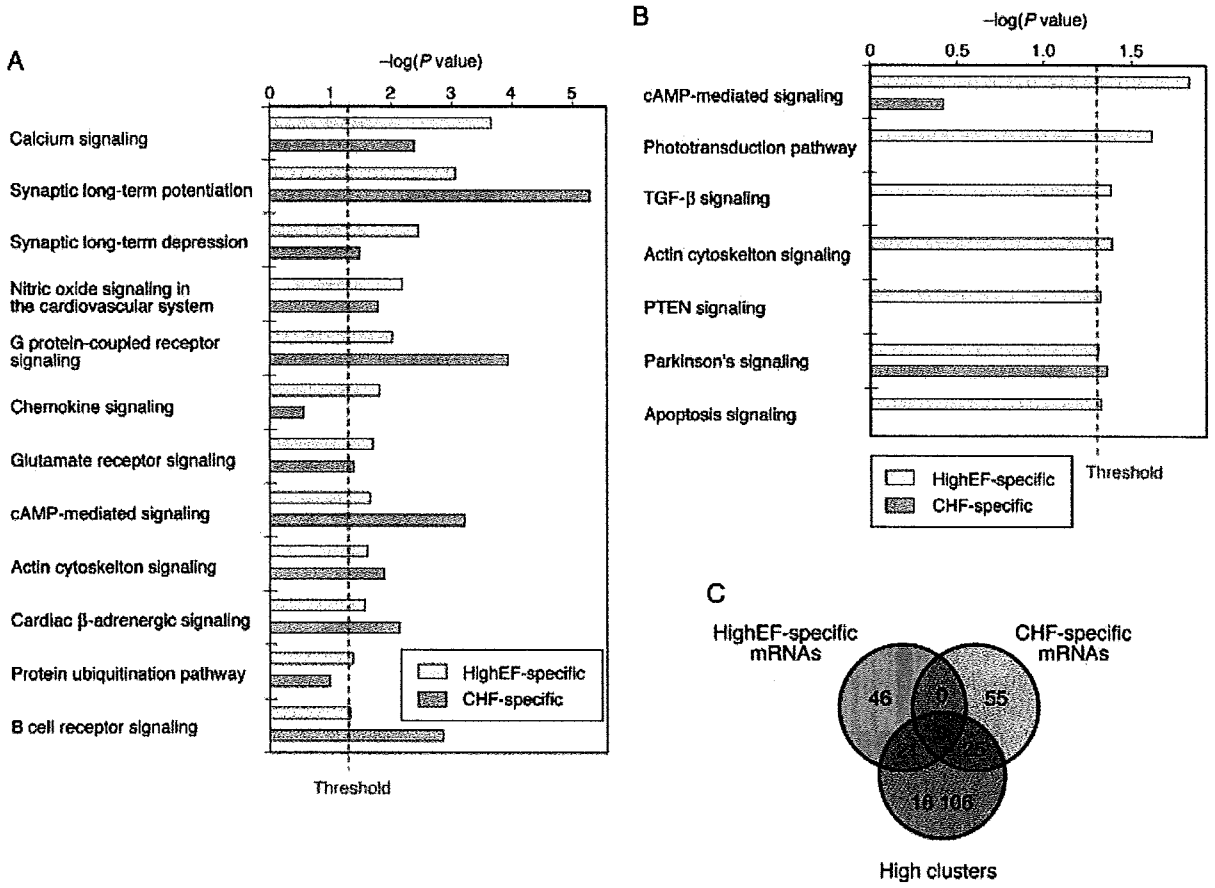

Figure 3 Analysis of genes that map in the vicinity of disease-dependent high clusters. (A) Canonical signaling pathways overrepresented in the HighEF-specific or CHF-specific high clusters for the K4TM ChIP products are listed with the corresponding −log(*P* value) score. (B) Canonical signaling pathways overrepresented in the HighEF-specific or CHF-specific high clusters for the K9TM ChIP products are listed with the corresponding −log(*P* value) score. (C) Venn diagram for comparison of transcripts associated specifically with HighEF or CHF status and those encoded by genes that map within a distance of < 5 kbp relative to a high cluster.

were widely distributed throughout human chromosomes and showed little overlap (see Fig. S3 in Supporting Information).

We examined whether the protein products of RefSeq genes that mapped in the vicinity (a distance of ≤ 5 kbp) of disease-dependent clusters function in canonical intracellular signaling pathways with the use of Ingenuity Pathway Analysis software (Ingenuity Systems; http://www.ingenuity.com). Analysis of the RefSeq genes associated with the disease-dependent K4TM clusters identified 12 canonical pathways that were significantly overrepresented ($P < 0.05$, Fisher's exact test) in HighEF-specific clusters and 20 pathways overrepresented in CHF-specific clusters. Many of the pathways ($n = 10$) were overrepresented in both HighEF-K4TM and CHF-K4TM clusters, almost all of which (including those for calcium signaling, synaptic long-term regulation, and nitric oxide signaling) are related to cardiac function (Fig. 3A).

Consistent with the disease-dependent selection of the clusters, the HighEF-associated and CHF-associated genes were distinct even within the same pathways. The canonical pathway for synaptic long-term potentiation, for example, contains the products of eight HighEF-associated and 12 CHF-associated genes, the interactions among which are shown in Fig. S4 in Supporting Information. Although genes corresponding to the calmodulin complex are present in both gene sets, these genes differ between the HighEF set (*CALM1*) and the CHF set (*CALM3*).

In addition to the proteins of the canonical signaling pathways, many products of the genes in the vicinity of disease-dependent high clusters for K4TM are functionally or physically networked. One such network comprises 34 proteins, 18 of which are encoded by HighEF-associated genes and 16 by CHF-associated genes (Fig. S5 in Supporting Information). Again, the genes for some complexes associated with both gene sets are distinct; those for the ATPase complex, for instance, include that for ATP1B1 in the HighEF-associated set and that for ATP5C1 in the CHF-associated set. Gene products in this network are substantially enriched in those implicated in cardiovascular disease.

In contrast to the K4TM-specific clusters, only a few canonical signaling pathways are linked to the RefSeq genes localized in the vicinity of K9TM-specific clusters. This difference is due in part to the small number of high clusters that contain disease-dependent reads for K9TM. Whereas the numbers of high clusters for HighEF specimens were similar between K4TM and K9TM products ($n = 6547$ and 5594, respectively), the numbers of disease-dependent clusters for the K9TM mark were only approximately 25% of those for the K4TM mark (Table 2). Seven canonical signaling pathways were over-represented ($P < 0.05$, Fisher's exact test) in the genes associated with the HighEF-K9TM clusters, whereas only one such pathway was overrepresented in those associated with the CHF-K9TM clusters (Fig. 3B). The network containing the most disease-dependent K9TM-associated gene products is centered on transforming growth factor β1 (TGFB1) and the tumor suppressor p53 (TP53), implicating K9TM-related regulation in cell death in the heart (see Fig. S6 in Supporting Information).

Our analysis thus revealed differential regulation of K4TM modification for genes related to cardiac function. To examine whether such epigenetic regulation plays a direct role in gene transcription, we performed gene expression profiling with Human Genome U133 Plus 2.0 arrays (Affymetrix) for the individual specimens (four for HighEF and four for CHF) used in the ChIP experiments. From the data obtained for 54 675 probe sets and the eight specimens, we selected HighEF-specific probe sets according to the following criteria: (i) the ratio of the mean expression level between HighEF and CHF was ≥ 3, and (ii) the mean expression level in HighEF was ≥ 10 arbitrary units (U). These criteria resulted in the isolation of 67 probe sets (see Table S3 in Supporting Information). CHF-specific probe sets were also selected on the basis of a CHF/HighEF ratio for mean expression level of ≥ 3 and a mean expression level in CHF of ≥ 10 U, resulting in the identification of 80 probe sets (see Table S4 in Supporting Information). A total of 16 152 of the transcripts measured with the U133 Plus 2.0 arrays mapped within a distance of ≤ 5 kbp relative to the high clusters. A Venn diagram revealed that only 21 probe sets were shared between the HighEF-specific and high cluster–associated transcripts, whereas 25 probe sets were shared between the CHF-specific and high cluster–associated transcripts (Fig. 3C). The K4TM mark has been found to map preferentially to the transcription start sites of active genes (Bernstein *et al.* 2005). Although a typical correlation between the K4TM modification and selective gene expression was apparent for a subset of genes (Fig. 4), our results suggest that this dynamic epigenetic regulation in the heart may not always directly participate in transcriptional regulation of neighboring genes.

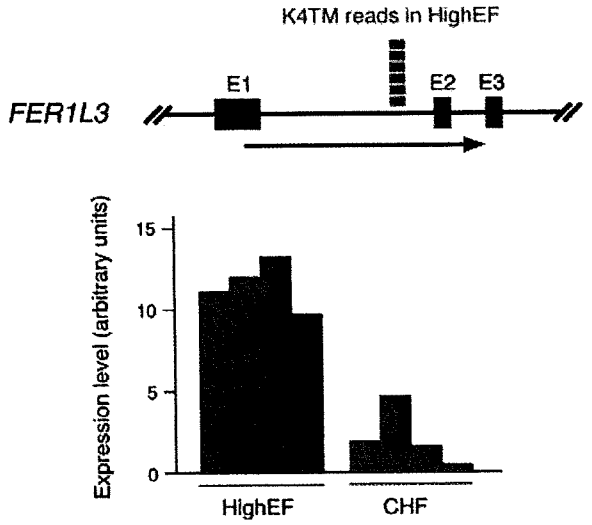

Figure 4 Epigenetic profile and mRNA abundance for *FER1L3*. Six sequence reads were selectively identified in the first intron of the *FER1L3* gene for the K4TM ChIP products of the HighEF sample (upper panel). E, exon. Consistent with this epigenetic profile, the amount of *FER1L3* mRNA was higher in the HighEF specimens than in the CHF specimens, as judged from the microarray data (lower panel).

Discussion

In the present study, we have revealed heart failure–dependent changes in the epigenetic profiles for K4TM and K9TM marks. The antibodies used in this study have been utilized in other reports for ChIP experiments, with those for K4TM and K9TM being especially employed in a genome-wide epigenetic profiling (Pokholok *et al.* 2005; Vakoc *et al.* 2006). Although it is difficult to

extensively verify our data in this study (because of the lack of knowledge in epigenetic profiles in heart), our ChIP procedure could faithfully confirm the epigenetic data demonstrated in previous studies [You *et al.* have, for instance, revealed that an apicidin treatment decreases the K4TM level while increases the K9TM level in the exon 1 of *DNMT1* in HeLa cells (You *et al.* 2008), and we could observe similar changes in the same experiment (data not shown)], supporting the reliability of our ChIP procedures.

Despite increasing evidence for a role of histone acetylation-deacetylation in the development of cardiac hypertrophy and heart failure, little information has been available for other histone modifications in these conditions (Illi *et al.* 2005; Phan *et al.* 2005; Bingham *et al.* 2007). Given the marked differences between the profiles of dimethylation and trimethylation for both K4 and K9 sites of histone H3, such trimethylation is likely under strict regulation in failed hearts.

The genes positioned close to the K4TM or K9TM marks were highly enriched in those that encode components of signaling pathways related to cardiac function. The HighEF-specific K4TM modification was, for instance, associated with *RYR2*, *CACNA2D1*, and *CACNB2* genes, the products of which directly participate in the regulation of intracellular calcium concentration and in muscle contraction (Cataldi *et al.* 1999; Marx *et al.* 2000). However, such disease-dependent histone methylation was not always linked to the induction or repression of neighboring genes. The expression level of the above three genes thus did not differ significantly between HighEF and CHF specimens (data not shown). Furthermore, only ~30% of HighEF- or CHF-specific transcripts were derived from genes associated with disease-dependent K4TM or K9TM modification (Fig. 3C). Consistent with such observations, the expression ratio for probe sets between normal and failed hearts of Dahl rats was not significantly correlated with the intensity ratio for any of the examined histone modifications, including H3Ac and H4Ac (data not shown). Therefore, despite the marked association between disease status and both transcript abundance and a subset of histone modifications, none of the latter can directly account for the former.

The epigenetic changes associated with heart failure may regulate gene transcription not through a single modification but through a combination of various marks (the "histone code" hypothesis) (Strahl & Allis 2000). The disease-dependent epigenetic changes also may alter the conformation of chromosomes, inducing an open or closed chromatin structure that indirectly affects the targets of subsequent regulation, such as the binding of transcription factors or additional chromatin remodeling. The subsequent regulation step would then play an important role in transcription of neighboring genes. In either case, our epigenetic profiles should facilitate further investigations into the roles of epigenetic changes in the development of heart failure.

Experimental procedures

ChIP-on-chip experiments

Dahl salt-sensitive rats (Japan SLC) at 6 weeks of age were maintained on a low-sodium diet (0.3% NaCl) or switched to a high-sodium diet (8% NaCl); the latter animals developed heart failure, as detected by echocardiography, after 13 weeks, as described previously (Ueno *et al.* 2003). ChIP products were prepared from the LV myocytes of 19-week-old Dahl rats with antibodies specific to H3Ac (Upstate, #17-245), H4Ac (Upstate, #17-229), K4DM (Abcam, #ab7766), K4TM (Abcam, #ab8580), K9DM (Upstate, #07-441), K9TM (Upstate, #07-442), K20TM (Abcam, #ab9053) or K27DM (Upstate, #07-452). The products were amplified by T7 RNA polymerase and subjected to hybridization with Affymetrix Rat Genome 230 2.0 microarrays as described previously (Takayama *et al.* 2007). Total genomic DNA (Pre-ChIP) and cRNA prepared from the LV tissue were also hybridized to the same arrays. The mean expression intensity of all probe sets was set to 500 U in each hybridization, and the fluorescence intensity of each test gene was normalized accordingly. Microarray data for rat and human hearts are available at the Gene Expression Omnibus web site (http://www.ncbi.nlm.nih.gov/geo) under the accession numbers GSE8341 and GSE8331, respectively. For the ChIP data, the signal intensity of each probe set in the Pre-ChIP analysis was then subtracted from that of the corresponding probe set in each ChIP experiment.

ChIP-to-seq experiments

All clinical specimens were obtained with written informed consent, and the study was approved by the ethics committees of Jichi Medical University and Hayama Heart Center. ChIP products were prepared from pooled samples for HighEF or CHF (each derived from four specimens) with antibodies to K4TM or K9TM. The products were converted to cRNA and amplified as described above for ChIP-on-chip experiments. The cRNA was then used to generate double-stranded DNA, which was subjected to pyrosequencing with a Genome Sequencer 20 system (Roche Diagnostics). Keypass wells occupied 82.7% to 87.0% of original Raw wells. Homology searches with the BLAST program were performed against the human genome sequence (the hg18 assembly) for each readout with the following parameter set: –e 2e-19 –v 50 –b 500 –T F –F F –m 8.

Acknowledgements

This work was supported in part by a Grant-in-Aid for Scientific Research on Priority Areas (C) "Medical Genome Science" from the

Ministry of Education, Culture, Sports, Science and Technology of Japan and by a grant (#04C7) from Salt Science Research Foundation (Tokyo, Japan).

References

Bernstein, B.E., Kamal, M., Lindblad-Toh, K., Bekiranov, S., Bailey, D.K., Huebert, D.J., McMahon, S., Karlsson, E.K., Kulbokas, E.J. 3rd, Gingeras, T.R., Schreiber, S.L. & Lander, E.S. (2005) Genomic maps and comparative analysis of histone modifications in human and mouse. *Cell* **120**, 169–181.

Bingham, A.J., Ooi, L., Kozera, L., White, E. & Wood, I.C. (2007) The repressor element 1-silencing transcription factor regulates heart-specific gene expression using multiple chromatin-modifying complexes. *Mol. Cell. Biol.* **27**, 4082–4092.

Braunwald, E. (1997) Shattuck lecture—cardiovascular medicine at the turn of the millennium: triumphs, concerns, and opportunities. *N. Engl. J. Med.* **337**, 1360–1369.

Cataldi, M., Secondo, A., D'Alessio, A., Taglialatela, M., Hofmann, F., Klugbauer, N., Di Renzo, G. & Annunziato, L. (1999) Studies on maitotoxin-induced intracellular $Ca^{(2+)}$ elevation in Chinese hamster ovary cells stably transfected with cDNAs encoding for L-type $Ca^{(2+)}$ channel subunits. *J. Pharmacol. Exp. Ther.* **290**, 725–730.

Gusterson, R.J., Jazrawi, E., Adcock, I.M. & Latchman, D.S. (2003) The transcriptional co-activators CREB-binding protein (CBP) and p300 play a critical role in cardiac hypertrophy that is dependent on their histone acetyltransferase activity. *J. Biol. Chem.* **278**, 6838–6847.

Iezzi, S., Di Padova, M., Serra, C., Caretti, G., Simone, C., Maklan, E., Minetti, G., Zhao, P., Hoffman, E.P., Puri, P.L. & Sartorelli, V. (2004) Deacetylase inhibitors increase muscle cell size by promoting myoblast recruitment and fusion through induction of follistatin. *Dev. Cell* **6**, 673–684.

Illi, B., Scopece, A., Nanni, S., Farsetti, A., Morgante, L., Biglioli, P., Capogrossi, M.C. & Gaetano, C. (2005) Epigenetic histone modification and cardiovascular lineage programming in mouse embryonic stem cells exposed to laminar shear stress. *Circ. Res.* **96**, 501–508.

James, M.A., Saadeh, A.M. & Jones, J.V. (2000) Wall stress and hypertension. *J. Cardiovasc. Risk* **7**, 187–190.

Kuwahara, K., Saito, Y., Ogawa, E., Takahashi, N., Nakagawa, Y., Naruse, Y., Harada, M., Hamanaka, I., Izumi, T., Miyamoto, Y., Kishimoto, I., Kawakami, R., Nakanishi, M., Mori, N. & Nakao, K. (2001) The neuron-restrictive silencer element-neuron-restrictive silencer factor system regulates basal and endothelin 1-inducible atrial natriuretic peptide gene expression in ventricular myocytes. *Mol. Cell. Biol.* **21**, 2085–2097.

Marx, S.O., Reiken, S., Hisamatsu, Y., Jayaraman, T., Burkhoff, D., Rosemblit, N. & Marks, A.R. (2000) PKA phosphorylation dissociates FKBP12.6 from the calcium release channel (ryanodine receptor): defective regulation in failing hearts. *Cell* **101**, 365–376.

Phan, D., Rasmussen, T.L., Nakagawa, O., McAnally, J., Gottlieb, P.D., Tucker, P.W., Richardson, J.A., Bassel-Duby, R. & Olson, E.N. (2005) BOP, a regulator of right ventricular heart development, is a direct transcriptional target of MEF2C in the developing heart. *Development* **132**, 2669–2678.

Pokholok, D.K., Harbison, C.T., Levine, S., Cole, M., Hannett, N.M., Lee, T.I., Bell, G.W., Walker, K., Rolfe, P.A., Herbolsheimer, E., Zeitlinger, J., Lewitter, F., Gifford, D.K. & Young, R.A. (2005) Genome-wide map of nucleosome acetylation and methylation in yeast. *Cell* **122**, 517–527.

Rapp, J.P., Wang, S.M. & Dene, H. (1989) A genetic polymorphism in the renin gene of Dahl rats cosegregates with blood pressure. *Science* **243**, 542–544.

Santos-Rosa, H., Schneider, R., Bannister, A.J., Sherriff, J., Bernstein, B.E., Emre, N.C., Schreiber, S.L., Mellor, J. & Kouzarides, T. (2002) Active genes are tri-methylated at K4 of histone H3. *Nature* **419**, 407–411.

Strahl, B.D. & Allis, C.D. (2000) The language of covalent histone modifications. *Nature* **403**, 41–45.

Takayama, K., Kaneshiro, K., Tsutsumi, S., Horie-Inoue, K., Ikeda, K., Urano, T., Ijichi, N., Ouchi, Y., Shirahige, K., Aburatani, H. & Inoue, S. (2007) Identification of novel androgen response genes in prostate cancer cells by coupling chromatin immunoprecipitation and genomic microarray analysis. *Oncogene* **26**, 4453–4463.

Ueno, S., Ohki, R., Hashimoto, T., Takizawa, T., Takeuchi, K., Yamashita, Y., Ota, J., Choi, Y.L., Wada, T., Koinuma, K., Yamamoto, K., Ikeda, U., Shimada, K. & Mano, H. (2003) DNA microarray analysis of *in vivo* progression mechanism of heart failure. *Biochem. Biophys. Res. Commun.* **307**, 771–777.

Vakoc, C.R., Sachdeva, M.M., Wang, H. & Blobel, G.A. (2006) Profile of histone lysine methylation across transcribed mammalian chromatin. *Mol. Cell. Biol.* **26**, 9185–9195.

You, J.S., Kang, J.K., Lee, E.K., Lee, J.C., Lee, S.H., Jeon, Y.J., Koh, D.H., Ahn, S.H., Seo, D.W., Lee, H.Y., Cho, E.J. & Han, J.W. (2008) Histone deacetylase inhibitor apicidin downregulates DNA methyltransferase 1 expression and induces repressive histone modifications via recruitment of corepressor complex to promoter region in human cervix cancer cells. *Oncogene* **27**, 1376–1386.

Zhang, C.L., McKinsey, T.A., Chang, S., Antos, C.L., Hill, J.A. & Olson, E.N. (2002) Class II histone deacetylases act as signal-responsive repressors of cardiac hypertrophy. *Cell* **110**, 479–488.

Received: 26 June 2008
Accepted: 10 October 2008

Supporting Information/Supplementary materials

The following Supporting Information can be found in the online version of the article:

Figure S1 Distribution of K4TM and K9TM marks on chromosome 1.

Figure S2 Distribution of read number per cluster in ChIP products.

Figure S3 Chromosome distribution of disease-specific high clusters.

Figure S4 Protein complexes in the synaptic long-term potentiation pathway in Fig. 3A are colored red or green on the basis of whether the corresponding genes are associated with HighEF-specific or CHF-specific high clusters for K4TM, respectively.

Figure S5 Interaction map for a protein network that contains the products of 18 and 16 genes associated with the HighEF-specific and CHF-specific high clusters for K4TM, respectively.

Figure S6 Network for the products of genes that mapped in the vicinity of K9TM high clusters.

Table S1 Output of pyrosequencing.

Table S2 High clusters identified in the heart specimens.

Table S3 Expression intensity of HighEF-specific probe sets.

Table S4 Expression intensity of CHF-specific probe sets.

Additional Supporting Information may be found in the online version of the article.

Please note: Wiley-Blackwell are not responsible for the content or functionality of any supporting information supplied by the authors. Any queries (other than missing material) should be directed to the corresponding author for the article.

Potential role of miR-29b in modulation of *Dnmt3a* and *Dnmt3b* expression in primordial germ cells of female mouse embryos

SHUJI TAKADA,[1,4] EUGENE BEREZIKOV,[2] YOUNG LIM CHOI,[1] YOSHIHIRO YAMASHITA,[1] and HIROYUKI MANO[1,3]

[1]Division of Functional Genomics, Jichi Medical University, 3311-1 Yakushiji, Shimotsukeshi, Tochigi 329-0498, Japan
[2]Hubrecht Institute, Uppsalalaan 8, Utrecht, The Netherlands
[3]Core Research for Evolution Science and Technology (CREST), Japan Science and Technology Agency, Saitama 332-0012, Japan

ABSTRACT

MicroRNAs (miRNAs) are a recently discovered class of small noncoding RNAs and are implicated in an increasing number of biological processes. To examine whether miRNAs might contribute to sexual differentiation, we performed expression profiling of miRNAs in mouse embryonic gonads with the use of a highly sensitive cloning method, mRAP. Our profiling data revealed substantial differences in the miRNA repertoire between male and female gonads at embryonic (E) day 13.5 (E13.5), suggesting that such differentially expressed miRNAs may function in sexual differentiation. Female-specific miRNAs included miR-29b, which also has been known to be expressed in a similar sex-dependent manner in the gonads of chicken embryos, suggestive of a conserved role in gonadogenesis. Transcripts of the human genes for the de novo methyltransferases DNMT3A and DNMT3B have been identified as targets of miR-29b, and we found that mouse miR-29b also negatively regulates *Dnmt3a* and *Dnmt3b* expression in luciferase reporter assays. We also found that miR-29b is expressed in mouse primordial germ cells (PGCs) at E13.5 and that its expression is up-regulated in a female-specific manner between E13.5 and E17.5, when male-specific de novo methylation of the PGC genome is known to occur. Our data thus suggest that miR-29b may play an important role in female gonadal development by targeting *Dnmt3a* and *Dnmt3b* and thereby modulating methylation of genomic DNA in PGCs.

Keywords: mRAP; microRNA; mouse; chicken; gonad; primordial germ cell

INTRODUCTION

MicroRNAs (miRNAs) are short noncoding RNAs of 20–24 nucleotides (nt) that negatively regulate protein production from target mRNAs. They function by interacting with their target mRNAs through incomplete base-pairing to the 3′ untranslated region (3′UTR) (Filipowicz 2005; Hammond 2005; Hannon 2002; Mattick and Makunin 2005) and thereby either trigger degradation of the target mRNAs or suppress their translation. MicroRNAs have been identified in a wide range of organisms, including plants and animals (Carrington and Ambros 2003; Bartel 2004). Many miRNAs are conserved throughout evolution, but substantial diversity is also apparent for some miRNAs even between closely related species (Berezikov et al. 2006a).

Expression of miRNAs has been shown to be tightly regulated in a developmental stage-dependent, as well as in an organ-dependent, manner (Aboobaker et al. 2005; Wienholds et al. 2005; Ason et al. 2006; Kloosterman et al. 2006; Takada et al. 2006a), suggesting that they may play important roles in embryonic development and tissue organization. The miRNAs miR-1 and miR-124, for example, are specifically expressed in muscle and the central nervous system, respectively, in zebrafish, medaka, mouse, and fly, suggesting that the function of these miRNAs is conserved across animal phyla (Kloosterman and Plasterk 2006).

Although the precise function of most miRNAs remains unclear, some have been shown to contribute to a variety of biological phenomena, including intracellular signaling, apoptosis, metabolism, cardiogenesis, myogenesis, and brain development (Kloosterman and Plasterk 2006). Essential roles for miRNAs in animal development have been revealed

[4]**Present address:** Department of Systems BioMedicine, National Institute for Child Health and Development, 2-10-1 Okura, Setagaya, Tokyo, Japan 157-8535.
Reprint requests to: Shuji Takada, Department of Systems BioMedicine, National Institute for Child Health and Development, 2-10-1 Okura, Setagaya, Tokyo, Japan 157-8535; e-mail: stakada@nch.go.jp; fax: 81-3-3417-2498.
Article published online ahead of print. Article and publication date are at http://www.rnajournal.org/cgi/doi/10.1261/rna.1418309.

by analysis of cells deficient in Dicer, an enzyme required for the production of miRNAs from their precursors. *Dicer* null mutant mice thus die in utero at embryonic (E) day 7.5 (E7.5) and lack stem cell compartments (Bernstein et al. 2003). Mice with conditional ablation of this gene have also revealed that Dicer (and, therefore, probably also miRNAs) is required for morphogenesis of the limb (Harfe et al. 2005), skin (Andl et al. 2006; Yi et al. 2006), and lung epithelium (Harris et al. 2006). However, the genes targeted by miRNAs to achieve their effects remain largely unknown.

The heterogametic pairing of the sex chromosomes, X and Y, results in male development in mammals, whereas females are the heterogametic sex (ZW) in birds. Despite this difference in sex determination, several important genes for sexual differentiation are expressed in a similar manner in the gonads of both mammals and birds, suggesting the existence of a shared mechanism for this process. In mammals, the gonads first emerge as bipotential organs that subsequently develop into testes or ovaries depending on whether *Sry*, a sex-determining gene on the Y chromosome, is expressed or not (Gubbay et al. 1990; Koopman et al. 1991).

Identification of a function for miRNAs in mammalian gonadal development would be facilitated by characterization of miRNA expression profiles in developing gonads. However, most current technologies for measurement of miRNA expression either require substantial amounts of RNA for analysis (in the case of conventional cloning methods) or are unable to examine unknown miRNA species (in the case of microarray- or stem–loop-based detection methods). Neither of these types of approach is, therefore, suitable for extensive miRNA profiling of the gonads, for which only small quantities of tissue are usually available and many unknown miRNAs may be present.

We have recently developed a highly sensitive cloning procedure for miRNAs (Mano and Takada 2007; Takada et al. 2006a; Takada and Mano 2007). This procedure, designated miRNA amplification profiling (mRAP), allows the isolation of tens of thousands of miRNA clones from small quantities of starting material (even from as few as 10,000 cells). Coupling of mRAP to a computational pipeline in order to detect or predict miRNAs thus represents an optimal means for quantitative measurement of miRNA expression profiles in small amounts of tissue or clinical specimens. We have now applied such technology to mouse gonads in order to identify sex-dependent expression of miRNAs.

RESULTS

miRNA expression profiling of mouse embryonic gonads

To identify miRNAs expressed differentially between male and female mouse gonads at E13.5, we constructed small RNA-derived cDNA libraries by the mRAP protocol from these tissues. Totals of 672 and 1440 cDNA concatamers were sequenced, resulting in the identification of 1153 and 1480 small RNA sequences, for male and female embryonic gonads, respectively. Totals of 180 and 184 of these sequences from male and female gonad libraries, respectively, matched known miRNAs (Table 1). In addition, three candidates for novel miRNAs (miR-143*, miR-715*, miR-689*) were identified, each of which is present in the hairpin structure of known miRNAs. The remaining small RNA sequences likely represent RNA degradation products.

Identification of miRNAs that are expressed in a sex-dependent manner at E13.5

We have previously shown that mRAP cloning frequency reflects relative miRNA abundance in cells, provided that sufficient numbers of small RNA-derived cDNAs are sequenced (Takada et al. 2006a; S Takada and H Mano, unpubl.). In the current data set, many miRNAs were found to be expressed in a sex-dependent manner. For instance, the most abundant miRNA in both sexes, miR-29b, is preferentially expressed (by a factor of ~2) in the female gonad (Table 1).

To confirm such sexually differential expression of miRNAs, we performed Northern blot analysis. The abundance of miR-29b normalized by that of U6 RNA was 2.3 arbitrary units (U) in the female gonad and 1.0 U in the male gonad at E13.5 (Fig. 1), consistent with the mRAP data (read counts of 73.0% and 30.4% for female and male, respectively) (Table 1). In contrast, the fourth most abundant miRNA, miR-143, was found to be preferentially expressed in male gonads by both Northern blot analysis (1.7 versus 1.0 U in male and female, respectively) (Fig. 1) and mRAP analysis (8.70% versus 0.51%) (Table 1), although the male-to-female ratio differed between the two approaches. The sex-related expression of other miRNAs (miR-24, miR-142-3p, miR-126-5p) revealed by mRAP was not detected by Northern analysis (Fig. 1). Together, these data thus showed that certain miRNAs are expressed in the gonads in a sex-dependent manner.

Expression patterns of miR-29b and miR-143 during sexual differentiation

With the use of Northern blot analysis, we next examined the expression profiles of the sex-specific miRNAs miR-29b and miR-143 during mouse gonadogenesis. In the female gonad, expression of miR-29b was increased at E15.5 compared with that at E13.5, and the increased level of expression was maintained through E17.5 (Fig. 2). In the male gonad, the relative abundance of miR-29b increased gradually from E13.5 to E17.5 but was consistently lower than that in stage-matched female gonads, suggesting that miR-29b may play different roles in male and female gonads.

TABLE 1. Profiling of miRNAs by mRAP in mouse embryonic gonads at E13.5

miRNA	Read counts (%)[a] Male	Female
mmu-mir-29b	56 (30.43)	143 (72.96)
mmu-mir-142-3p	28 (15.22)	8 (4.08)
mmu-mir-124	14 (7.61)	5 (2.55)
mmu-mir-143	16 (8.70)	1 (0.51)
mmu-mir-689	1 (0.54)	11 (5.61)
mmu-mir-24	9 (4.89)	1 (0.51)
mmu-mir-1	5 (2.72)	2 (1.02)
mmu-mir-126-5p	4 (2.17)	1 (0.51)
mmu-let-7c	3 (1.63)	1 (0.51)
mmu-mir-142-5p	2 (1.09)	2 (1.02)
mmu-let-7b	1 (0.54)	3 (1.53)
mmu-mir-143*	4 (2.17)	0 (0)
mmu-mir-19b	2 (1.09)	2 (1.02)
mmu-mir-191	3 (1.63)	0 (0)
mmu-mir-146a	1 (0.54)	2 (1.02)
mmu-mir-351	3 (1.63)	0 (0)
mmu-let-7g	2 (1.09)	0 (0)
mmu-mir-541	2 (1.09)	0 (0)
mmu-mir-194	2 (1.09)	0 (0)
mmu-mir-126-3p	2 (1.09)	0 (0)
mmu-mir-30c	2 (1.09)	0 (0)
mmu-mir-130a	1 (0.54)	1 (0.51)
mmu-mir-217	2 (1.09)	0 (0)
mmu-mir-145	1 (0.54)	1 (0.51)
mmu-mir-99b	1 (0.54)	1 (0.51)
mmu-mir-30b	2 (1.09)	0 (0)
mmu-mir-28*	0 (0)	2 (1.02)
mmu-mir-141	2 (1.09)	0 (0)
mmu-mir-715*	0 (0)	1 (0.51)
mmu-mir-223	1 (0.54)	0 (0)
mmu-mir-136*	0 (0)	1 (0.51)
mmu-mir-29c	1 (0.54)	0 (0)
mmu-mir-19a	0 (0)	1 (0.51)
mmu-mir-184	1 (0.54)	0 (0)
mmu-mir-27b	1 (0.54)	0 (0)
mmu-mir-27a	1 (0.54)	0 (0)
mmu-mir-301a	0 (0)	1 (0.51)
mmu-mir-715	0 (0)	1 (0.51)
mmu-mir-298	0 (0)	1 (0.51)
mmu-mir-30a	1 (0.54)	0 (0)
mmu-mir-378	1 (0.54)	0 (0)
mmu-mir-744	1 (0.54)	0 (0)
mmu-mir-33	0 (0)	1 (0.51)
mmu-mir-125a-5p	1 (0.54)	0 (0)
mmu-mir-125b-5p	1 (0.54)	0 (0)
mmu-mir-139-5p	1 (0.54)	0 (0)
mmu-mir-92a	1 (0.54)	0 (0)
mmu-mir-214	1 (0.54)	0 (0)
mmu-mir-122	0 (0)	1 (0.51)
mmu-mir-689*	0 (0)	1 (0.51)
Total	184 (100)	196 (100)

[a]Cloning frequency of each miRNA in the library was expressed as a percentage of the total counts for all miRNA reads in each organ.

The expression of miR-143 in the male gonad increased from E13.5 to E15.5 but decreased to an intermediate level at E17.5 (Fig. 2). In contrast, the relative amount of miR-143 increased gradually between E13.5 and E17.5 in the female gonad, suggesting that this miRNA might have a specific function in male gonadogenesis at E15.5.

Evolutionary conservation of miR-29b and miR-143 expression

If miR-29b or miR-143 contributes directly to sex-dependent differentiation of the gonads in mice, their expression profiles might be expected to be evolutionarily conserved. This has been, indeed, shown in the cases for *Sox9*, *Amh*, and *FoxL2*, all of which are essential for sexual differentiation of the gonads (Carre-Eusebe et al. 1996; Kent et al. 1996; Morais da Silva et al. 1996; Loffler et al. 2003). We therefore examined the expression of miR-29b and miR-143 in chicken embryonic gonads during sexual differentiation with Northern blot analysis using male and female chicken embryonic gonads. The right and left gonads were treated separately, because there is a left–right asymmetry associated with the chicken gonadal differentiation. The relative abundance of miR-29b was greater in female gonads than in male gonads of chicken embryos at days 12 and 18 (Fig. 3), an expression profile similar to that apparent for mouse gonads (Fig. 2). In contrast, the expression of miR-143 was greater in male than in female chicken gonads at day 18 (Fig. 3). The preferential expression of miR-143 in male gonads was thus confirmed in chicken in a similar pattern to that in mouse (Fig. 2).

Identification of cell types in which miR-29b and miR-143 are expressed

We next investigated which cells express miR-29b or miR-143 in the gonads of mouse embryos. To determine

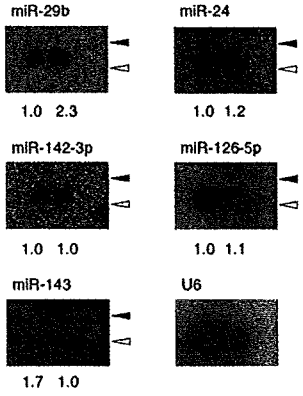

FIGURE 1. Validation of mRAP data by Northern blot analysis. Fractions containing small RNAs (0.5–0.8 μg per lane) isolated from (*left* lanes) male or (*right* lanes) female mouse gonads at E13.5 were subjected to Northern analysis with LNA probes specific for the indicated miRNAs or U6 RNA. The signal intensity for each miRNA normalized by that of U6 RNA is shown at the *bottom* of each lane. (Closed and open arrowheads) The positions corresponding to 24 and 19 nt, respectively.

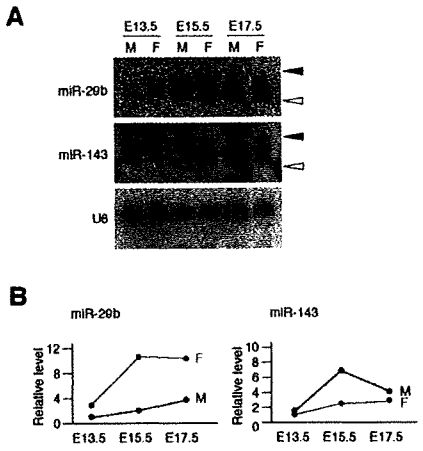

FIGURE 2. Sex-dependent expression profiles of miR-29b and miR-143 in mouse embryos. (*A*) Fractions containing small RNAs isolated from male (M) or female (F) mouse gonads at E13.5, E15.5, or E17.5 were subjected to Northern blot analysis with probes specific for miR-29b, miR-143, or U6 RNA. (Closed and open arrowheads) The positions corresponding to 24 and 19 nt, respectively. (*B*) The hybridization signal intensity for each miRNA in *A* was normalized by that of U6 RNA and plotted against embryonic stage.

whether such expression is restricted to somatic or germ cells, we performed Northern blot analysis with RNA isolated from embryos exposed in utero to busulfan, which is known to eliminate germ cells (Forsberg and Olivecrona 1966). Depletion of germ cells in busulfan-treated mouse gonads was confirmed by measurement of the expression of *Oct4* that is restricted to primordial germ cells (PGCs) in both testis and ovary at E13.5 (Pesce et al. 1998). Whole-mount in situ hybridization thus revealed the presence of *Oct4* mRNA in E13.5 mouse gonads exposed to DMSO vehicle but not in those exposed to busulfan (Fig. 4A).

Northern blot analysis with an LNA probe for miR-29b detected a discrete signal with RNA recovered from DMSO-treated female gonads, whereas the signal was mostly lost with RNA from those treated with busulfan (Fig. 4B), indicating that miR-29b is expressed exclusively in PGCs in female embryonic gonads. Although miR-143 was also found to be preferentially expressed in PGCs, a substantial amount of this miRNA remained in busulfan-treated male gonads, suggesting that miR-143 may be expressed in both somatic cells and PGCs of the testis.

Target genes of miR-29b in mouse PGCs

Our findings that miR-29b is expressed almost exclusively in PGCs of female gonads and that the expression profile of this miRNA is conserved between mouse and chicken suggests that miR-29b function is likely important for PGCs in female gonads. The genes for DNA methyltransferases 3A (DNMT3A) and 3B (DNMT3B) were recently shown to be direct targets of miR-29b, and overexpression of this miRNA results in a reduction in the global level of DNA methylation in the human genome (Fabbri et al. 2007). Given that mouse *Dnmt3a* and *Dnmt3b* are expressed in PGCs at E12.5–E17.5 (Lees-Murdock et al. 2005), these genes are candidates for regulation by miR-29b in mouse PGCs. Indeed, the TargetScan program (Lewis et al. 2003; Grimson et al. 2007), an in silico approach to the prediction of miRNA targets, indicated that both *Dnmt3a* and *Dnmt3b* are potential targets of this mouse miRNA (Fig. 5A). We, therefore, examined whether *Dnmt3a* or *Dnmt3b* is regulated by miR-29b in mouse.

To this end, we utilized a luciferase reporter assay. As a host cell line, using Northern blot analysis we searched for a cell line in which miR-29b does not exist; however, such a cell line was not found (data not shown). Since transfection efficiency of NIH3T3 is high, we used this cell line as a host cell. DNA fragments corresponding to portions of the 3′UTRs of *Dnmt3a* or *Dnmt3b* mRNAs containing the predicted miR-29b target sites were inserted into the 3′UTR of firefly luciferase cDNA, and the resulting reporter plasmids were introduced with or without miR-29b into NIH3T3 fibroblasts. The same target sequences but with a 1-base-pair (bp) mismatch were similarly inserted into the luciferase cDNA to yield negative control constructs (Fig. 5A). The luciferase activities of the constructs with the wild-type target regions of *Dnmt3a* or *Dnmt3b* were reduced compared with those of the corresponding mutant

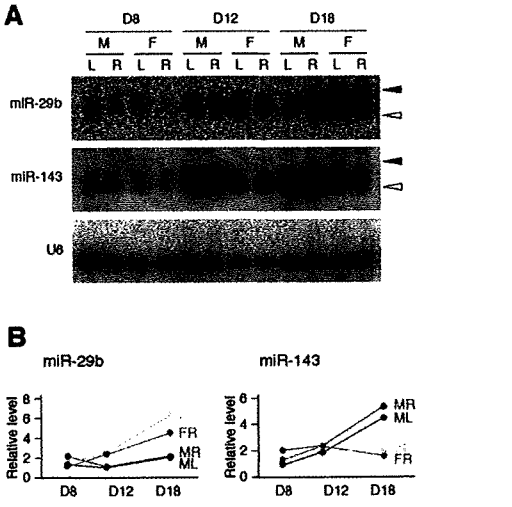

FIGURE 3. Sex-specific up-regulation of miR-29b and miR-143 expression in chicken embryos. (*A*) Fractions containing small RNAs isolated from male (M) or female (F) chicken gonads at day (D) 8, 12, or 18 were subjected to Northern blot analysis with probes specific for miR-29b, miR-143, or U6 RNA. (L) Left gonad; (R) right gonad. (Closed and open arrowheads) The positions corresponding to 24 and 19 nt, respectively. (*B*) The hybridization signal intensity for each miRNA in *A* was normalized by that of U6 RNA and plotted against embryonic stage. (ML) Male left gonad; (MR) male right gonad; (FL) female left gonad; (FR) female right gonads.

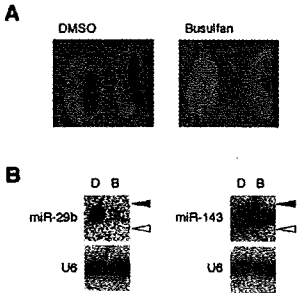

FIGURE 4. Expression of miR-29b and miR-143 in PGCs of mouse embryos at E13.5. (*A*) Male (M) and female (F) embryonic gonads were recovered at E13.5 from dams injected with DMSO or busulfan and were subjected to whole-mount in situ hybridization with a probe specific for *Oct4* mRNA. (*B*) Fractions containing small RNAs isolated from female or male gonads treated as in *A* were subjected to Northern blot analysis with probes specific for miR-29b or miR-143, respectively. The same blots were also subjected to hybridization with a probe specific for U6 RNA. (Closed and open arrowheads) The positions corresponding to 24 and 19 nt, respectively. Embryos exposed to (D) DMSO or (B) busulfan.

constructs (Fig. 5B), likely because miR-29b is expressed in NIH3T3 cells (data not shown). Furthermore, the luciferase activities of the wild-type constructs for *Dnmt3a* or *Dnmt3b* were reduced by cotransfection with miR-29b, whereas those of the mutant constructs were not (Fig. 5B). These results thus suggested that both genes may be targets of miR-29b in mouse.

DISCUSSION

We have determined the miRNA expression profiles of male and female embryonic mouse gonads at E13.5. Given that most conventional methods for cloning of miRNAs require >100 μg of total RNA (Lagos-Quintana et al. 2002), it would have been difficult to profile miRNA expression in embryonic gonads by such approaches with the small amounts of tissue available. We therefore adopted mRAP, a cloning- and sequencing-based method with a high sensitivity, for miRNA profiling in embryonic gonads.

We obtained a total of 380 miRNA-derived sequences, consisting of 374 reads for known miRNAs and six reads for previously unreported ones (four corresponding to miR-143*, one to miR-715*, and one to miR-689*). Although 2000 mRAP clones were sequenced in the present study, most of the miRNAs (both known and novel) in our data set were detected five or fewer times (Table 1), indicating that all miRNAs in the gonads may not yet have been identified. Extensive sequencing of mRAP clones may therefore result in the identification of additional novel hairpin structures containing unreported miRNA candidates.

We found that miR-29b is the most abundant miRNA in mouse gonads at E13.5. Northern blot analysis of PGC-depleted gonadal tissue further indicated that miR-29b is expressed almost exclusively in PGCs of female gonads (at least at E13.5). This finding contrasts with results of Hayashi et al. (2008) showing that miR-29b was virtually undetectable in mouse PGCs at this stage by RT-PCR analysis. This discrepancy may be attributable to the differences in methodology or in genetic background of the mice between the two studies.

Although the differences in mRAP cloning frequency between male and female gonads for some miRNAs were reflected in differences in expression as determined by Northern blot analysis, those for others were not. We have recently performed deep sequencing of mRAP clones from various mouse organs and found that the correlation between cloning frequency and Northern blot data was dependent on miRNA sequence (S Takada and H Mano, unpubl.). Even some miRNAs with a read number of >100,000 per organ were not detected by Northern blot analysis. The nucleotide sequence of miRNAs may thus greatly affect their sensitivity to detection by Northern blot analysis or by RT-PCR (a hybridization-based detection system). However, it remains possible that mRAP may have a cloning bias for some miRNAs.

Both *Dnmt3a* and *Dnmt3b* are expressed in mouse PGCs of both sexes at E13.5 (Lees-Murdock et al. 2005), suggesting

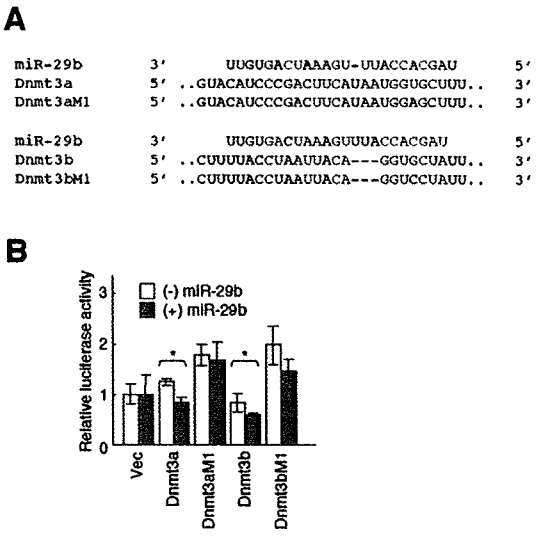

FIGURE 5. Identification of *Dnmt3a* and *Dnmt3b* as potential targets of miR-29b in mouse. (*A*) Potential target sites for miR-29b in the 3′UTRs of *Dnmt3a* and *Dnmt3b* mRNAs are shown aligned with the miR-29b sequence. The same 3′UTR sequences with a 1-bp mismatch (M1) were used as negative controls in luciferase reporter assays. Complementary bases between miR-29b (red) and the 3′UTRs (blue) are shown, respectively. (*B*) Luciferase reporter assays were performed with vectors containing DNA fragments corresponding to the putative wild-type or mutant target sites for miR-29b in the 3′UTRs of *Dnmt3a* or *Dnmt3b* mRNAs. The assays were performed in NIH3T3 cells cotransfected (or not) with the miR-29b precursor. Vec indicates cells transfected with the luciferase vector without *Dnmt3* sequences. Firefly luciferase activity was normalized by that of *Renilla* luciferase, and the data are means ± SD from three independent experiments. (*) $P < 0.05$ for the indicated comparisons (Student's *t*-test).

a possibility that DNA methylation of the genome is regulated by miR-29b. Methylation of cytosine residues is the only known direct epigenetic modification of mammalian genomic DNA and contributes to various biological phenomena including transposon silencing and genomic imprinting (Reik et al. 2001; Bird 2002). There are two main types of DNA methyltransferase: maintenance methyltransferases that methylate hemimethylated CpG sequences after DNA replication, and de novo methyltransferases that methylate cytosine residues of unmethylated CpG sequences, and which include DNMT3A and DNMT3B (Okano et al. 1998). Genome-wide demethylation occurs early during development and is complete around E13 to E14 in PGCs of both male and female mouse embryos (Monk et al. 1987; Kafri et al. 1992; Brandeis et al. 1993; Surani 1998; Tada et al. 1998). Re-methylation then takes place earlier in the male germ cells (from E15 to E16) (Kafri et al. 1992; Brandeis et al. 1993; Coffigny et al. 1999) than in the female cells (after birth, during the growth of oocytes) (Lucifero et al. 2002, 2004; Hiura et al. 2006). DNMT3A and DNMT3B were recently shown to mediate de novo methylation of differentially methylated genomic regions corresponding to imprinted genes and some repetitive elements in male germ cells (Kato et al. 2007). It is thus possible that the expression of these two enzymes is repressed by miR-29b in female germ cells, allowing an escape from male-type methylation of the genome and underlying female-type methylation.

MicroRNAs have been shown to contribute to the fine-tuning of physiological events or to function as molecular switches in cellular signaling (Lee et al. 1993; Wightman et al. 1993; Moss et al. 1997; Reinhart et al. 2000; Brennecke et al. 2003; Johnston and Hobert 2003; Sokol and Ambros 2005). In addition, some miRNAs function in a fail-safe mechanism to silence mRNAs that are unwanted in specific cell types (Hornstein et al. 2005; Cohen et al. 2006). It seems likely that miR-29b may function in such a mechanism to regulate methylation of the genome, given that the amount of *Dnmt3a* mRNA in PGCs is similar in male and female mouse embryos at E13.5 but is greater in male than in female PGCs at E15.5 and E17.5 (Iwahashi et al. 2007).

Further extensive sequencing of mRAP clones from the gonads will provide additional insight into the cell type-dependent and developmental stage-dependent expression profiles of miRNAs, and such information will likely contribute to understanding of the function of miRNAs in sex determination and differentiation.

MATERIALS AND METHODS

Mice and tissues

C57BL/6J mice (*Mus musculus domesticus*) were obtained from a local supplier (Japan SLC). The mice were allowed to mate naturally, and at noon of the day in which a vaginal plug was observed were considered to be E0.5. Gonads depleted of germ cells were prepared by intraperitoneal injection of pregnant females at E9.5 with 100 μL of a warmed solution (16 mg/mL) of busulfan (Sigma-Aldrich) in 50% dimethly sulfoxide (DMSO), and harvesting of the embryos occurred on E13.5 (Forsberg and Olivecrona 1966); as a control, dams were injected with 50% DMSO alone. The sex of each embryo was determined on the basis of the presence (male) or absence (female) of a testis cord.

Chickens and tissues

Fertilized chicken (*Gallus gallus domestica*) eggs were obtained from a local supplier (Saitama Experimental Animal Supply) and were maintained at 18°C until their transfer to an incubator at 37.8°C. Staging of chicken embryos was confirmed at dissection as described by Hamburger and Hamilton (1951). The gonads of each embryo were snap frozen, and the sex of the embryos was determined as described previously (Clinton et al. 2001; Takada et al. 2006b,c) with the use of a polymerase chain reaction (PCR)-based method performed with genomic DNA extracted from the hind limbs.

mRAP

The mRAP procedure was performed as described previously (Takada et al. 2006a; Mano and Takada 2007; Takada and Mano 2007), and miRNAs were identified from mRAP clones with the use of the computational pipeline developed by Berezikov et al. (2006b).

Northern blot analysis

A fraction of small RNA molecules (<200 nt) was prepared with the use of a mirVana miRNA Isolation Kit (Applied Biosystems), and portions of the fraction (0.5–0.8 μg per lane) were subjected to electrophoresis on a 15% polyacrylamide gel under denaturing conditions. The separated RNA molecules were transferred electrophoretically to a Hybond-N membrane (GE Healthcare UK) and were subjected to hybridization with the use of the ULTRAhyb-Oligo reagent (Applied Biosystems) and with ^{32}P-labeled locked nucleic acid (LNA) probes corresponding to reverse complementary sequences of mature miRNAs. Signals were detected with a BAS-1500 image analyzer (Fuji Photo Film), and signal intensities were measured with the use of Image Gauge version 4.1 software (Fuji Photo Film). The signal intensities of the miRNAs were normalized to that of U6 RNA. Probes included:

mmu-miR-29bRCLNA (5′-AAcACtGAtTTcAAaTGgTGcTA-3′) for miR-29b;
mmu-miR-142-3pRCLNA (5′-CCaTAaAGtAGgAAaCAcTAcA-3′) for miR-142-3p;
mmu-miR-143RCLNA (5′-TGaGCtACaGTgCTtCAtCTcA-3′) for miR-143;
mmu-miR-24RCLNA (5′-CTgTTcCTgCTgAAcTGaGCcA-3′) for miR-24;
mmu-miR-126-5pRCLNA (5′-CgCGtACcAAAAGtAAtAAtG-3′) for miR-126-5p; and
U6AS (5′-AACGCTTCACGAATTTGCGT-3′) for U6 RNA.

Here, upper- and lowercase letters designate DNA and LNA, respectively.

Whole-mount in situ hybridization

Whole-mount in situ hybridization was performed by the maleic acid buffer (MABT) method as previously described (Xu and Wilkinson 1998). A probe for *Oct4* mRNA was prepared from total RNA isolated from E12.5 mouse embryos. The RNA was subjected to reverse transcription (RT), and the resulting cDNA was subjected to PCR with the primers mOct4probe1F (5′-GCC TTGCAGCTCAGCCTTAAGA-3′) and mOct4probe1R (5′-CCTC GCCCTCAGGAAAAGGGAC-3′). The amplification product, which corresponds to the probe described by Thomas et al. (1998), was cloned into the pGEM-T Easy vector (Promega) for production of the probe by in vitro transcription.

Luciferase assay

DNA fragments corresponding to a 981-bp portion of the 3′UTR of *Dnmt3a* or a 637-bp portion of the 3′UTR of *Dnmt3b* were amplified by PCR from C57BL/6J mouse genomic DNA. The primers wereDnmt3aAmpF (5′-ACTAGTGACTGAAACAAGAGA GTTA-3′) and Dnmt3aAmpR (5′-ACGCGTGGACCGGAGCTGC CATGTGC-3′) for *Dnmt3a* and Dnmt3bAmpF (5′-ACTAGTGG TACAAGGGCTGAAGTCC-3′) and Dnmt3bAmpR (5′-ACGCGT AAGGCAGTCTCTCCCCACAC-3′) for *Dnmt3b*, with the underlined sequences corresponding to recognition sites for restriction endonucleases. The PCR products were cloned into pGEM-T Easy and verified by nucleotide sequencing. Single nucleotide substitutions were introduced into the DNA sequences with the use of a QuikChange Multi Site-Directed Mutagenesis Kit (Stratagene) and the primers Dnmt3aM1 (5′-GACTTCATAATGGAGCTTT CAAAACAG-3′) for *Dnmt3a* and Dnmt3bM1 (5′-ACCTAATTA CAGGTCCTATTTTATAG-3′) for *Dnmt3b*, with the underlined residues corresponding to the substituted bases. The insert of each clone was subcloned into the SpeI and MluI sites of the multiple cloning region of the pMIR-Report-luciferase vector (Applied Biosystems). The coding sequence and 3′UTR of the firefly luciferase cDNA as well as the insert of each of the resulting vectors were then subcloned into the BamHI and NotI sites of the pMXS vector (kindly provided by T. Kitamura, Institute of Medical Science, University of Tokyo).

NIH3T3 cells grown in 24-well plates were transfected with 50 μM miR-29b precursor (Pre-miR miRNA Precursor Molecule; Applied Biosystems), 0.6 μg of pMXS-based luciferase reporter vector, and 0.2 μg of a control *Renilla* luciferase vector (pRL-TK; Promega) in the presence of the Lipofectamine 2000 reagent (Invitrogen). Firefly and *Renilla* luciferase activities in cell lysates were assayed with the use of a Dual-Luciferase Reporter Assay System (Promega) 48 h after cell transfection, and the former activity was normalized by the latter.

ACKNOWLEDGMENTS

We thank the laboratory members for their discussions, as well as M. Otani, K. Nakamura, and S. Aoyagi for technical assistance. This work was supported in part by Grants-in-Aid for Scientific Research from the Ministry of Education, Culture, Sports, Science and Technology of Japan (to S.T.); a grant for Third-Term Comprehensive Control Research for Cancer from the Ministry of Health, Labor, and Welfare of Japan (to H.M.); and a grant for Scientific Research on Priority Areas "Applied Genomics" from the Ministry of Education, Culture, Sports, Science and Technology of Japan (to H.M.).

Received October 14, 2008; accepted April 27, 2009.

REFERENCES

Aboobaker AA, Tomancak P, Patel N, Rubin GM, Lai EC. 2005. *Drosophila* microRNAs exhibit diverse spatial expression patterns during embryonic development. *Proc Natl Acad Sci* **102:** 18017–18022.

Andl T, Murchison EP, Liu F, Zhang Y, Yunta-Gonzalez M, Tobias JW, Andl CD, Seykora JT, Hannon GJ, Millar SE. 2006. The miRNA-processing enzyme dicer is essential for the morphogenesis and maintenance of hair follicles. *Curr Biol* **16:** 1041–1049.

Ason B, Darnell DK, Wittbrodt B, Berezikov E, Kloosterman WP, Wittbrodt J, Antin PB, Plasterk RH. 2006. Differences in vertebrate microRNA expression. *Proc Natl Acad Sci* **103:** 14385–14389.

Bartel DP. 2004. MicroRNAs: Genomics, biogenesis, mechanism, and function. *Cell* **116:** 281–297.

Berezikov E, Thuemmler F, van Laake LW, Kondova I, Bontrop R, Cuppen E, Plasterk RH. 2006a. Diversity of microRNAs in human and chimpanzee brain. *Nat Genet* **38:** 1375–1377.

Berezikov E, van Tetering G, Verheul M, van de Belt J, van Laake L, Vos J, Verloop R, van de Wetering M, Guryev V, Takada S, et al. 2006b. Many novel mammalian microRNA candidates identified by extensive cloning and RAKE analysis. *Genome Res* **16:** 1289–1298.

Bernstein E, Kim SY, Carmell MA, Murchison EP, Alcorn H, Li MZ, Mills AA, Elledge SJ, Anderson KV, Hannon GJ. 2003. Dicer is essential for mouse development. *Nat Genet* **35:** 215–217.

Bird A. 2002. DNA methylation patterns and epigenetic memory. *Genes & Dev* **16:** 6–21.

Brandeis M, Kafri T, Ariel M, Chaillet JR, McCarrey J, Razin A, Cedar H. 1993. The ontogeny of allele-specific methylation associated with imprinted genes in the mouse. *EMBO J* **12:** 3669–3677.

Brennecke J, Hipfner DR, Stark A, Russell RB, Cohen SM. 2003. *bantam* encodes a developmentally regulated microRNA that controls cell proliferation and regulates the proapoptotic gene *hid* in *Drosophila*. *Cell* **113:** 25–36.

Carre-Eusebe D, di Clemente N, Rey R, Pieau C, Vigier B, Josso N, Picard JY. 1996. Cloning and expression of the chick anti-Müllerian hormone gene. *J Biol Chem* **271:** 4798–4804.

Carrington JC, Ambros V. 2003. Role of microRNAs in plant and animal development. *Science* **301:** 336–338.

Clinton M, Haines L, Belloir B, McBride D. 2001. Sexing chick embryos: A rapid and simple protocol. *Br Poult Sci* **42:** 134–138.

Coffigny H, Bourgeois C, Ricoul M, Bernardino J, Vilain A, Niveleau A, Malfoy B, Dutrillaux B. 1999. Alterations of DNA methylation patterns in germ cells and Sertoli cells from developing mouse testis. *Cytogenet Cell Genet* **87:** 175–181.

Cohen SM, Brennecke J, Stark A. 2006. Denoising feedback loops by thresholding—A new role for microRNAs. *Genes & Dev* **20:** 2769–2772.

Fabbri M, Garzon R, Cimmino A, Liu Z, Zanesi N, Callegari E, Liu S, Alder H, Costinean S, Fernandez-Cymering C, et al. 2007. MicroRNA-29 family reverts aberrant methylation in lung cancer by targeting DNA methyltransferases 3A and 3B. *Proc Natl Acad Sci* **104:** 15805–15810.

Filipowicz W. 2005. RNAi: The nuts and bolts of the RISC machine. *Cell* **122:** 17–20.

Forsberg JG, Olivecrona H. 1966. The effect of prenatally administered Busulphan on rat gonads. *Biol Neonat* **10:** 180–192.

Grimson A, Farh KK, Johnston WK, Garrett-Engele P, Lim LP, Bartel DP. 2007. MicroRNA targeting specificity in mammals: Determinants beyond seed pairing. *Mol Cell* **27:** 91–105.

Gubbay J, Collignon J, Koopman P, Capel B, Economou A, Münsterberg A, Vivian N, Goodfellow P, Lovell-Badge R. 1990.

A gene mapping to the sex-determining region of the mouse Y chromosome is a member of a novel family of embryonically expressed genes. *Nature* **346:** 245–250.

Hamburger V, Hamilton HL. 1951. A series of normal stages in the development of the chick embryo. *J Morphol* **88:** 49–92.

Hammond SM. 2005. Dicing and slicing: The core machinery of the RNA interference pathway. *FEBS Lett* **579:** 5822–5829.

Hannon GJ. 2002. RNA interference. *Nature* **418:** 244–251.

Harfe BD, McManus MT, Mansfield JH, Hornstein E, Tabin CJ. 2005. The RNaseIII enzyme Dicer is required for morphogenesis but not patterning of the vertebrate limb. *Proc Natl Acad Sci* **102:** 10898–10903.

Harris KS, Zhang Z, McManus MT, Harfe BD, Sun X. 2006. Dicer function is essential for lung epithelium morphogenesis. *Proc Natl Acad Sci* **103:** 2208–2213.

Hayashi K, Chuva de Sousa Lopes SM, Kaneda M, Tang F, Hajkova P, Lao K, O'Carroll D, Das PP, Tarakhovsky A, Miska EA, et al. 2008. MicroRNA biogenesis is required for mouse primordial germ cell development and spermatogenesis. *PLoS One* **3:** e1738. doi: 10.1371/journal.pone.0001738.

Hiura H, Obata Y, Komiyama J, Shirai M, Kono T. 2006. Oocyte growth-dependent progression of maternal imprinting in mice. *Genes Cells* **11:** 353–361.

Hornstein E, Mansfield JH, Yekta S, Hu JK, Harfe BD, McManus MT, Baskerville S, Bartel DP, Tabin CJ. 2005. The microRNA miR-196 acts upstream of Hoxb8 and Shh in limb development. *Nature* **438:** 671–674.

Iwahashi K, Yoshioka H, Low EW, McCarrey JR, Yanagimachi R, Yamazaki Y. 2007. Autonomous regulation of sex-specific developmental programming in mouse fetal germ cells. *Biol Reprod* **77:** 697–706.

Johnston RJ, Hobert O. 2003. A microRNA controlling left/right neuronal asymmetry in *Caenorhabditis elegans*. *Nature* **426:** 845–849.

Kafri T, Ariel M, Brandeis M, Shemer R, Urven L, McCarrey J, Cedar H, Razin A. 1992. Developmental pattern of gene-specific DNA methylation in the mouse embryo and germ line. *Genes & Dev* **6:** 705–714.

Kato Y, Kaneda M, Hata K, Kumaki K, Hisano M, Kohara Y, Okano M, Li E, Nozaki M, Sasaki H. 2007. Role of the Dnmt3 family in de novo methylation of imprinted and repetitive sequences during male germ cell development in the mouse. *Hum Mol Genet* **16:** 2272–2280.

Kent J, Wheatley SC, Andrews JE, Sinclair AH, Koopman P. 1996. A male-specific role for SOX9 in vertebrate sex determination. *Development* **122:** 2813–2822.

Kloosterman WP, Plasterk RH. 2006. The diverse functions of microRNAs in animal development and disease. *Dev Cell* **11:** 441–450.

Kloosterman WP, Wienholds E, de Bruijn E, Kauppinen S, Plasterk RH. 2006. In situ detection of miRNAs in animal embryos using LNA-modified oligonucleotide probes. *Nat Methods* **3:** 27–29.

Koopman P, Gubbay J, Vivian N, Goodfellow P, Lovell-Badge R. 1991. Male development of chromosomally female mice transgenic for Sry. *Nature* **351:** 117–121.

Lagos-Quintana M, Rauhut R, Yalcin A, Meyer J, Lendeckel W, Tuschl T. 2002. Identification of tissue-specific microRNAs from mouse. *Curr Biol* **12:** 735–737.

Lee RC, Feinbaum RL, Ambros V. 1993. The *C. elegans* heterochronic gene *lin-4* encodes small RNAs with antisense complementarity to *lin-14*. *Cell* **75:** 843–854.

Lees-Murdock DJ, Shovlin TC, Gardiner T, De Felici M, Walsh CP. 2005. DNA methyltransferase expression in the mouse germ line during periods of de novo methylation. *Dev Dyn* **232:** 992–1002.

Lewis BP, Shih IH, Jones-Rhoades MW, Bartel DP, Burge CB. 2003. Prediction of mammalian microRNA targets. *Cell* **115:** 787–798.

Loffler KA, Zarkower D, Koopman P. 2003. Etiology of ovarian failure in blepharophimosis ptosis epicanthus inversus syndrome: FOXL2 is a conserved, early-acting gene in vertebrate ovarian development. *Endocrinology* **144:** 3237–3243.

Lucifero D, Mertineit C, Clarke HJ, Bestor TH, Trasler JM. 2002. Methylation dynamics of imprinted genes in mouse germ cells. *Genomics* **79:** 530–538.

Lucifero D, Mann MR, Bartolomei MS, Trasler JM. 2004. Gene-specific timing and epigenetic memory in oocyte imprinting. *Hum Mol Genet* **13:** 839–849.

Mano H, Takada S. 2007. mRAP, a sensitive method for determination of microRNA expression profiles. *Methods* **43:** 118–122.

Mattick JS, Makunin IV. 2005. Small regulatory RNAs in mammals. *Hum Mol Genet* **14:** R121–R132.

Monk M, Boubelik M, Lehnert S. 1987. Temporal and regional changes in DNA methylation in the embryonic, extraembryonic and germ cell lineages during mouse embryo development. *Development* **99:** 371–382.

Morais da Silva S, Hacker A, Harley V, Goodfellow P, Swain A, Lovell-Badge R. 1996. Sox9 expression during gonadal development implies a conserved role for the gene in testis differentiation in mammals and birds. *Nat Genet* **14:** 62–68.

Moss EG, Lee RC, Ambros V. 1997. The cold shock domain protein LIN-28 controls developmental timing in *C. elegans* and is regulated by the *lin-4* RNA. *Cell* **88:** 637–646.

Okano M, Xie S, Li E. 1998. Cloning and characterization of a family of novel mammalian DNA (cytosine-5) methyltransferases. *Nat Genet* **19:** 219–220.

Pesce M, Wang X, Wolgemuth DJ, Schöler H. 1998. Differential expression of the Oct-4 transcription factor during mouse germ cell differentiation. *Mech Dev* **71:** 89–98.

Reik W, Dean W, Walter J. 2001. Epigenetic reprogramming in mammalian development. *Science* **293:** 1089–1093.

Reinhart BJ, Slack FJ, Basson M, Pasquinelli AE, Bettinger JC, Rougvie AE, Horvitz HR, Ruvkun G. 2000. The 21-nucleotide *let-7* RNA regulates developmental timing in *Caenorhabditis elegans*. *Nature* **403:** 901–906.

Sokol NS, Ambros V. 2005. Mesodermally expressed *Drosophila* microRNA-1 is regulated by Twist and is required in muscles during larval growth. *Genes & Dev* **19:** 2343–2354.

Surani MA. 1998. Imprinting and the initiation of gene silencing in the germ line. *Cell* **93:** 309–312.

Tada T, Tada M, Hilton K, Barton SC, Sado T, Takagi N, Surani MA. 1998. Epigenotype switching of imprintable loci in embryonic germ cells. *Dev Genes Evol* **207:** 551–561.

Takada S, Mano H. 2007. Profiling of microRNA expression by mRAP. *Nat Protocols* **2:** 3136–3145.

Takada S, Berezikov E, Yamashita Y, Lagos-Quintana M, Kloosterman WP, Enomoto M, Hatanaka H, Fujiwara S, Watanabe H, Soda M, et al. 2006a. Mouse microRNA profiles determined with a new and sensitive cloning method. *Nucleic Acids Res* **34:** e115. doi: 10.1093/nar/gkl653.

Takada S, Ota J, Kansaku N, Yamashita H, Izumi T, Ishikawa M, Wada T, Kaneda R, Choi YL, Koinuma K, et al. 2006b. Nucleotide sequence and embryonic expression of quail and duck Sox9 genes. *Gen Comp Endocrinol* **145:** 208–213.

Takada S, Wada T, Kaneda R, Choi YL, Yamashita Y, Mano H. 2006c. Evidence for activation of Amh gene expression by steroidogenic factor 1. *Mech Dev* **123:** 472–480.

Thomas PQ, Brown A, Beddington RS. 1998. Hex: A homeobox gene revealing peri-implantation asymmetry in the mouse embryo and an early transient marker of endothelial cell precursors. *Development* **125:** 85–94.

Wienholds E, Kloosterman WP, Miska E, Alvarez-Saavedra E, Berezikov E, de Bruijn E, Horvitz HR, Kauppinen S, Plasterk RH. 2005. MicroRNA expression in zebrafish embryonic development. *Science* **309:** 310–311.

Wightman B, Ha I, Ruvkun G. 1993. Posttranscriptional regulation of the heterochronic gene *lin-14* by *lin-4* mediates temporal pattern formation in *C. elegans*. *Cell* **75:** 855–862.

Xu Q, Wilkinson D. 1998. In situ hybridization of mRNA with hapten labelled probes. In *In situ hybridization: A practical approach*, 2nd ed. (ed. D Wilkinson), pp. 87–106. Oxford University Press, Oxford, UK.

Yi R, O'Carroll D, Pasolli HA, Zhang Z, Dietrich FS, Tarakhovsky A, Fuchs E. 2006. Morphogenesis in skin is governed by discrete sets of differentially expressed microRNAs. *Nat Genet* **38:** 356–362.

Screening for genetic abnormalities involved in ovarian carcinogenesis using retroviral expression libraries

TOMOAKI WADA[1,2], YOSHIHIRO YAMASHITA[1], YASUSHI SAGA[2], KAYOKO TAKAHASHI[2], KOJI KOINUMA[1], YOUNG LIM CHOI[1], RURI KANEDA[1], SHIN-ICHIRO FUJIWARA[1], MANABU SODA[1], HIDEKI WATANABE[1], KENTARO KURASHINA[1], HISASHI HATANAKA[1], MUNEHIRO ENOMOTO[1], SHUJI TAKADA[1], HIROYUKI MANO[1,3] and MITSUAKI SUZUKI[2]

[1]Division of Functional Genomics and [2]Department of Obstetrics and Gynecology, School of Medicine, Jichi Medical University, Tochigi; [3]CREST, Japan Science and Technology Agency, Saitama, Japan

Received April 24, 2009; Accepted June 23, 2009

DOI: 10.3892/ijo_00000410

Abstract. The purpose of this study was to screen for genes involved in ovarian carcinogenesis in an attempt to develop an effective molecular-targeted therapy for ovarian cancer. We constructed retroviral expression libraries for the human ovarian cancer cell lines SHIN-3 and TYK-CPr, and performed a focus formation assay with 3T3 cells. As a result, *proteasome subunit beta-type 2 (PSMB2), ubiquitin-specific protease 14 (USP14)*, and *keratin 8 (KRT8)* were identified from SHIN-3, and *polymerase II RNA subunit (POLR2E), chaperonin containing T-complex polypeptide 1 subunit 4 (CCT4), glia maturation factor beta (GMFB)*, and *neuroblastoma ras viral oncogene homolog (NRAS)* from TYK-CPr. *NRAS* gene analysis revealed a CAA→AAA substitution at codon 61, resulting in a Glu→Lys change at position 61. When the mutant *NRAS* was introduced into fibroblasts for its expression, many transformed foci were generated, confirming the transforming ability of the mutant *NRAS*.

Introduction

Ovarian cancer is the fifth most common cause of death from gynecologic malignancies in the USA. Approximately 25,000 women are affected by ovarian cancer every year, and about 14,000 die of this disease (1). In recent years, debulking surgery followed by multidrug therapy with platinum and taxine drugs have been used, with some improvement in prognosis (2); however, the 5-year survival rate remains at about 50% (3). This is due to the lack of effective therapy for treatment-resistant or recurrent ovarian cancer.

A series of recent studies have reported that STI571, which targets the *BCR-ABL* gene responsible for chronic myelogenous leukemia, is effective for this disease, and that the anti-CD20 antibody rituximab is highly effective for B-cell lymphocytic leukemia (4). These observations have demonstrated that it is clinically very important to elucidate the pathogenesis of malignancies and thereby develop molecular-targeted therapy for them. To improve the prognosis of patients with ovarian cancer, it is important to define genetic abnormalities involved in the onset of this disease, and to develop effective molecular-targeted therapies for ovarian cancer.

To date, several studies have reported that mutations in the *p53* gene (5) or deletions in the *BRCA1* and *BRCA2* genes (6) are common in ovarian cancer. However, there is no evidence that these genetic abnormalities are directly involved in the development of ovarian cancer.

In a recent study, we constructed a full-length cDNA expression library of non-small cell lung cancer (NSCLC) using a retroviral vector, and demonstrated by functional screening that a fusion gene, composed of portions of the echinoderm microtubule-associated protein-like 4 (*EML4*) and anaplastic lymphoma kinase (*ALK*) genes, was involved in the development of NSCLC (7). In this study, we aimed to screen for genes responsible for ovarian carcinogenesis using similar techniques.

Materials and methods

Cell culture. Ovarian serous cystadenocarcinoma cell line SHIN-3 (8) and ovarian undifferentiated carcinoma cell line TYK-CPr (JCRB0234.1, Health Science Research Resources Bank: HSRRB, Osaka, Japan) (9) cells were cultured in Dulbecco's modified Eagle's medium/F12 (DMEM/F12; Invitrogen, Carlsbad, CA, USA) medium supplemented with 10% fetal bovine serum (Invitrogen), 2 mM L-glutamine (Invitrogen), and 1% penicillin-streptomycin (Invitrogen). The BOSC23 packaging cell line for ecotropic retroviruses (10) and mouse 3T3 fibroblasts (American Type Culture

Correspondence to: Dr Yasushi Saga, Department of Obstetrics and Gynecology, School of Medicine, Jichi Medical university, 3311-1 Yakushiji, Shimotsuke, Tochigi 329-0498, Japan
E-mail: saga@jichi.ac.jp

Key words: ovarian cancer, oncogene, retroviral expression screening, NRAS

Collection: ATCC) were maintained in DMEM/F12 supplemented with 10% fetal bovine serum and 2 mM L-glutamine, and 1% penicillin-streptomycin.

Construction of a retrovirus library. Total RNA was extracted from SHIN-3 and TYK-CPr cells with the use of an RNeasy Mini column and RNase-free DNase (Qiagen, Valencia, CA, USA), and first-strand cDNA was synthesized from the RNA with PowerScript reverse transcriptase, a SMART IIA oligonucleotide, and CDS primer IIA (Clontech, Palo Alto, CA, USA). The resulting cDNA molecules were then amplified for 15 cycles with the 5'-PCR primer IIA and a SMART PCR cDNA synthesis kit (Clontech), with the exception that LA Taq polymerase (Takara Bio, Shiga, Japan) was substituted for the Advantage 2 DNA polymerase provided with the kit. The PCR products were treated with proteinase K, rendered blunt-ended with T4 DNA polymerase, and ligated to a *BstXI* adapter (Invitrogen). Unbound adapters were removed with a cDNA size fractionation column (Invitrogen), and the modified cDNAs were ligated into the pMX retroviral plasmid (11) that had been digested with *BstXI*. The pMX-cDNA plasmids were introduced into ElecroMax DH10B cells (Invitrogen) by electroporation.

Focus formation assay. BOSC23 cells ($1.8x10^6$) were seeded onto 6-cm culture plates, cultured for 1 day, and then transfected with a mixture comprising 2 μg of retroviral plasmids, 0.5 μg of pGP plasmid (Takara Bio),.0.5 μg of pE-eco plasmid (Takara Bio), and 18 μl of Lipofectamine reagent (Invitrogen). Two days after transfection, polybrene (Sigma, St. Louis, MO, USA) was added at a concentration of 4 μg/ml to the culture supernatant, which was then used to infect 3T3 cells for 48 h. For the focus formation assay, the culture medium of 3T3 cells was changed to DMEM-high glucose (Invitrogen) supplemented with 5% calf serum and 2 mM L-glutamine. Transformed foci were isolated after 3 weeks of culture.

Recovery of cDNAs from 3T3 cells. Each 3T3 cell clone was harvested with a cloning syringe and cultured independently in a 10-cm culture plate. Genomic DNA was subsequently extracted from the cells and subjected to PCR with the 5'-PCR primer IIA and LA Taq polymerase for 50 cycles of 98°C for 20 sec and 68°C for 6 min. Amplified genomic fragments were purified by gel electrophoresis and ligated into the pT7Blue-2 vector (EMD Biosciences, San Diego, CA, USA) for nucleotide sequencing. The cDNAs obtained were introduced into the pMXS plasmid to prepare a recombinant retrovirus, which was used again to test its 3T3-transforming ability.

Analysis of the NRAS gene in the TYK-CPr cell line. Using as the substrate the cDNA that had been synthesized to construct the retroviral library, along with NRAS primers [5' primer (GTGGAGCTTGAGGTTCTTGC) and 3' primer (GCAG CTTGAAAGTGGCTCTT)], the *NRAS* gene was amplified by PCR for 30 cycles of 98°C for 30 sec, 62°C for 30 sec, and 68°C for 30 sec. The amplified DNA fragments were separated by electrophoresis, then purified, and inserted into the pGEM-T Easy Vector (Promega Corp., Madison, WI, USA) for sequencing.

Results

Construction of full-length cDNA expression libraries for SHIN-3 and TYK-CPr cells. cDNAs from SHIN-3 and TYK-CPr cells were inserted into the pMXS retroviral plasmid, which was then introduced into DH10B cells by electroporation. As a result, we obtained plasmid libraries of cDNA clones from SHIN-3 ($1.1x10^6$ colony-forming units, or cfu) and TYK-CPr ($1.2x10^6$ cfu) cells. From each of these plasmid clone libraries, 24 clones were picked up at random. In addition, to ascertain whether the cDNA inserts were full-length (complete reading frame), 10 clones were selected from each library, and ~500 bp of both ends of the cDNA insert were sequenced. The identified sequences were compared with the University of California-Santa Cruz Genome Browser Database (http://genome.ucsc.edu) by BLAST search (12). As a result, 7 of the 10 TYK-CPr-derived clones and 7 of the 10 SHIN-3-derived clones contained full-length cDNA inserts (data not shown). We therefore concluded that the retroviral cDNA expression libraries were of sufficient complexity and adequately enriched in full-length cDNAs for the present study.

Screening for transformed clones. 3T3 cells were transfected with retroviral cDNA expression libraries, and, after 3 weeks of culture, transformed clones were isolated. As a result, 17 and 15 transformed clones were identified for TYK-CPr and SHIN-3, respectively (Fig. 1).

Transformed clones were isolated using a cloning syringe, and cultured in separate dishes to extract genomic DNA from each clone. The genomic DNA was amplified by PCR using the same primers as those employed in cDNA amplification for library construction. As shown in Fig. 2, a single sharp cDNA band per clone was identified in about half of the clones.

Analysis of cDNAs recovered from transformed cells. Transformed clones, whose genomic DNA amplified by PCR gave a single sharp cDNA band, were selected, and their respective cDNAs were sequenced for gene identification. As a result, *proteasome subunit beta-type 2 (PSMB2), ubiquitin-specific protease 14 (USP14)*, and *keratin 8 (KRT8)* were identified from SHIN-3, and *polymerase II RNA subunit (POLR2E), chaperonin containing T-complex polypeptide 1 subunit 4 (CCT4), glia maturation factor beta (GMFB)*, and *neuroblastoma ras viral oncogene homolog (NRAS)* from TYK-CPr. All cDNAs contained complete open reading frames (ORF).

Analysis of the NRAS gene in the TYK-CPr cell line. Focusing on *NRAS* among the genes identified in this study, we examined the TYK-CPr-derived cDNA for point mutations, and found a codon 61 mutation (CAA→AAA, Glu→Lys) (Fig. 3).

Furthermore, the resulting mutant NRAS ($NRAS^{Q61K}$) cDNA was inserted into the pMX plasmid to construct a recombinant retrovirus, which was transfected into 3T3 cells for a focus formation assay. As shown in Fig. 4, the identified $NRAS^{Q61K}$ generated many transformed foci, confirming its transforming ability.

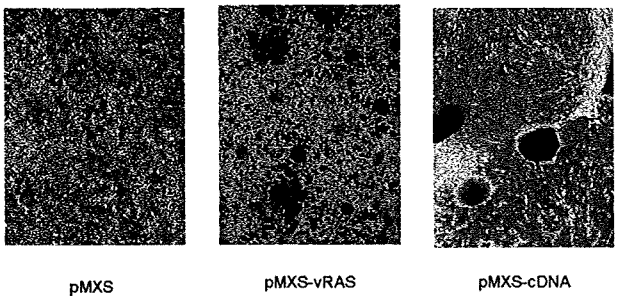

Figure 1. Focus formation assay with a retroviral library derived from TYK-CPr cells. Mouse 3T3 cells were infected with the empty virus (pMXS), a retrovirus expressing v-Ras as a positive control (pMXS-vRAS), or retroviruses from the TYK-CPr cell library (pMXS-cDNA). The cultures were photographed 3 weeks after infection.

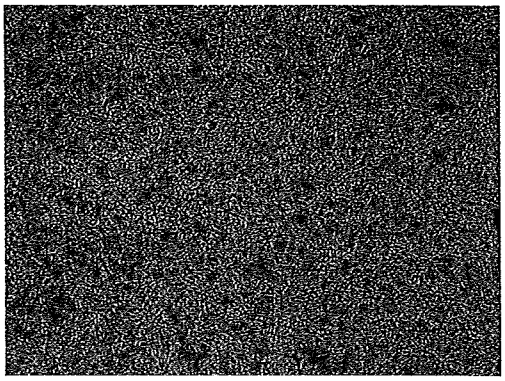

Figure 4. A recombinant retrovirus encoding NRAS^{Q61K} was used to infect 3T3 cells. The cells were photographed after culture for 2 weeks.

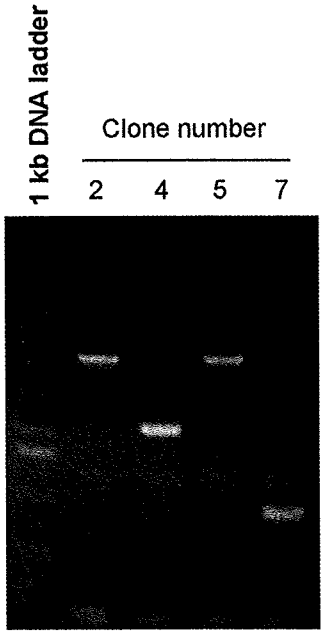

Figure 2. Genomic DNA isolated from transformed 3T3 cell foci (clone numbers 2, 4, 5, and 7) was subjected to PCR for amplification of the DNA inserts. The left lane contains DNA size markers (1-kbp DNA ladder; Invitrogen).

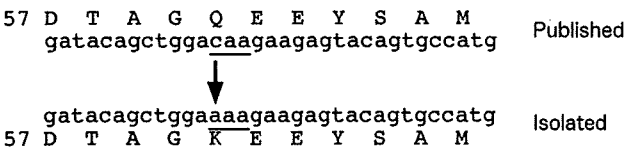

Figure 3. The amino acid sequence in the vicinity of the amino acid residue at position 61 of NRAS protein and the corresponding NRAS cDNA (NM_002524) codon sequence are shown in the upper row (published). Similarly, the amino acid sequence and the corresponding NRAS cDNA (isolated) codon sequence identified in this study are shown in the lower row. In the screened cDNA, the glutamine-encoding codon (caa) at position 61 had been converted to the lysine-encoding codon (aaa). The site of the nucleotide substitution is indicated in red.

To confirm that the NRAS^{Q61K} mutation did not arise during the process of library construction or PCR, we sequenced the *NRAS* gene in 10 randomly selected TYK-CPr cell clones, and found a CAA→AAA substitution at codon 61 in 7 clones. This indicates that the TYK-CPr cell line has a wild-type allele and a mutant allele (NRAS^{Q61K}).

Discussion

The focus formation assay in mouse 3T3 fibroblasts has been widely used to identify oncogenes (13). The conventional 3T3 focus formation assay involves the introduction of cancer cell-derived genomic DNA, followed by screening for focus-forming, transformed clones of 3T3 cells. To date, many oncogenes such as *RAS, ABL*, and *RAF* have been identified using this assay. However, the assay involving the introduction of genomic DNA alone has the major disadvantage of a lower screening ability, that is, the expression of oncogenes is controlled by their own enhancer/promoter region. However, the enhancer/promoter region of oncogenes functioning in ovarian cancer is not necessarily active in 3T3 fibroblasts. Therefore, the possibility of the successful identification of ovarian cancer-related oncogenes by the classical focus formation assay involving the introduction of genomic DNA alone is small. To ensure that all genes introduced into 3T3 cells are expressed at sufficient levels, it is necessary that their transcription be regulated by exogenous promoters and enhancers.

The retroviral vector is a type of vector most commonly used for gene introduction, and has advantages in that the cDNA inserted between the left and right long terminal repeats (LTR) is integrated directly into the chromosomes of infected cells, and viral vectors can be produced at high titers using packaging cells (14,15).

In this study, to screen for genes involved in ovarian carcinogenesis, we attempted to construct cDNA-expressing recombinant retroviral libraries that were engineered to express cDNA from retroviral LTR, and succeeded in constructing libraries with a sufficient complexity and mean insert size, derived from the ovarian cancer cell lines SHIN-3 and TYK-CPr. Using these libraries, we performed a focus formation assay in 3T3 cells, and were able to recover the cDNA inserts easily from the transformed clones employing the primers used for cDNA synthesis. From each of 7 clones, a single cDNA was identified and sequenced. As a result, *PSMB2, USP14*, and *KRT8* were screened from SHIN-3 cells, and *POLR2E, CCT4, GMFB*, and *NRAS* from TYK-CPr